# Intron retention as a new marker of the pre-disease state and its recovery to the normal state by a traditional Japanese multi-herbal medicine

Running title: Recovery of alternative splicing from the senescence to healthy type by an herbal medicine

**Norihiro Okada[a#], Kenshiro Oshima[a$], Yuki Iwasaki[a$], Akiko Maruko[a], Erica Iioka[a], Trieu-Duc Vu[a], Naoki Fujitsuka[b], Akinori Nishi[b], Aiko Sugiyama[b], Mitsue Nishiyama[b], Atsushi Kaneko[b], Masahiro Yamamoto[b] and Susumu Nishimura[ac]**

[a] Foundation for Advancement of International Science, 3-24-16 Kasuga, Tsukuba, Ibaraki 305-0821 Japan,
[b] Tsumura Kampo Research Laboratories, Tsumura & CO., 3586 Yoshiwara, Ami-machi, Ibaraki 300-1192 Japan,
[c] Laboratory Animal Resource Center, University of Tsukuba, 1-1-1 Tennodai, Tsukuba, Ibaraki 305-8575 Japan

[$] These two authors contributed equally to this work.
[#] To whom correspondence should be addressed.
nokada@fais.or.jp

Key words: RNA-seq, Kampo, senescence, alternative splicing, intron retention

Abbreviations: Cten: cell type enrichment analysis; DEG: differentially expressed genes; FC: fold change; GO: Gene Ontology; JTT: Juzen-taiho-to; IGV: Integrative Genomics Viewer; IR: intron retention; IJC: inclusion junction count; Kampo: Japanese multi-herbal medicines; KL: klotho mice; SJC: skipping junction count; RNA-seq: RNA sequencing; pre-mRNA: precursor mRNA; SE: skipped exon; TF: transcription factor; WT: wild type; 3-HBA: 3-hydroxybutyric acid

## Abstract

Intron retention (IR) is an important regulatory mechanism that affects gene expression and protein functions. Using klotho mice as a model, we proposed that retained introns are an excellent marker for the pre-disease state. Surprisingly, among widespread retained introns that accumulated during aging in the liver, a subset was recovered to the normal state by a Japanese traditional herbal medicine. IR-recovered genes fell into two categories: (1) those involved in the spliceosome and (2) those involved in liver-specific metabolism. By integrating data for splicing patterns, transcriptomes, and metabolomes, we hypothesize that this medicine-related IR recovery under the pre-disease state reflects the actual recovery of liver-specific function to the healthy state. Accordingly, the study provides proof-of-concept evidence related to the ancient Chinese statement proposing the medicine's usefulness for treating the pre-disease state. This approach lays out a method for elucidating unknown molecular mechanisms of an herbal medicine with multiple ingredients. (149 words)

## Introduction

The vast majority of precursor mRNAs (pre-mRNAs) in mammalian cells consists of exons separated by introns. Introns are normally removed by a mechanism called splicing, which leaves the joined exons that form the mature mRNA (Padgett et al., 1986, Patel and Steitz, 2003). The process of removing an intron from pre-mRNA is highly dynamic, during which a complex rearrangement of protein-protein, RNA-RNA, and RNA-protein interactions takes place in the spliceosome (Mayeda et al., 1994). Because of such complexity, the process is highly vulnerable to external stimuli (Stegeman and Weake, 2017). Dysregulation of RNA splicing has been identified as a causative defect in several diseases, especially in cancer (Dvinge et al., 2016).

It has recently become widely recognized among molecular biologists that aging reflects the gradual deterioration of the molecular components of the cell, the concerted functioning of which are vital for cell viability and proliferation (Lopez-Otin et al., 2013). In this sense, aging is regarded as a kind of disease, the extent of which varies among individuals. The complexity of alternative splicing of pre-mRNAs makes this process vulnerable even to aging, as suggested by many instances in which aging is accompanied by a change in the expression level of spliceosomal proteins or by a change in their splicing patterns (Zane et al., 2014). For example, levels of SF3B1 and

SRSF family proteins can be affected by changes in alternative splicing during aging (Deschenes and Chabot, 2017). As these changes in turn may alter the alternative splicing of numerous transcripts, a change in the expression of spliceosomal and associated proteins is primarily important.

Intron retention (IR) is one of the forms of alternative splicing and is considered to be harmful to the organism by (1) slowing down splicing kinetics to delay the onset of gene expression (Braunschweig et al., 2014), (2) increasing pre-mRNA degradation in the nucleus by nuclear exosomes (Niemela et al., 2014), and (3) increasing (pre-)mRNA degradation in the cytoplasm by nonsense-mediated decay (Lejeune and Maquat, 2005). IR accumulation has even been proposed as a post-transcriptional signature of aging (Adusumalli et al., 2019). Analyses of the transcriptome from mouse, human brain, and Drosophila head have shown a global increase in the level of IR during aging, indicating that this process may be evolutionarily conserved (Adusumalli et al., 2019).

In the present study, we used the klotho mouse, which is a model for senescence and exhibits a syndrome resembling human aging that includes a reduced life span, decreased activity, infertility, osteoporosis, atherosclerosis, atrophy of the skin, and emphysema (Kuro-o et al., 1997). This phenotype is caused by the disruption of a single gene, klotho (*Kl*). In a normal mouse, the klotho protein and FGF23 function as a receptor in the kidney to exert a diuretic action on phosphorus (Razzaque, 2009). In a klotho mouse, however, the blood level of phosphorus is very high because of a deficiency in the klotho protein, which leads to rapid senescence in this mouse.

Japanese multi-herbal medicines (Kampo) originated in ancient China and are widely used in Japan for various disorders. In contrast to chemically synthesized Western drugs, whose effects on humans are carefully evaluated during various stages of testing and whose mechanisms of actions are generally rigorously evaluated, it has been difficult to identify the molecular substances in the Kampo that are responsible for their potency and to analyze the mechanisms by which they exert their effects. It has long been said that thousands of chemical compounds in Kampo work together, sometimes synergistically, and that their side-effects, if any, are relatively minor, although their mechanism of action remains a total mystery (Zhou et al., 2016).

Juzen-taiho-to (JTT), being composed of 10 crude drugs as one of the formulations approved as a medicine in Japan, was first described in a drug textbook in the Song Dynasty (AD 1151) in China and was introduced in Japan during the Kamakura period (Saiki, 2000) (AD 1185−1333). It has been traditionally administered to patients with deficiency syndrome, consisting of disturbances and imbalances in the homeostatic condition of the body (Onishi et al., 1998). More specifically, it is prescribed for

108 patients with fatigue, anemia, night sweats, anorexia, or circulatory problems. JTT has
109 stimulatory effects on the immune response including enhancement of phagocytosis,
110 cytokine induction, induction of mitogenic activity of spleen cells, and activation of
111 macrophage and natural killer cells (Matsumoto et al., 2000). JTT can also prolong life
112 when combined with the surgical excision of tumors and has a protective effect against
113 the deleterious effects of chemotherapy drugs (Wang et al., 2018).
114 Knowing that aging can lead to an increase in retained introns, we used klotho mice
115 that had not yet undergone extensive aging and examined the effects of JTT on IR
116 patterns in genes expressed in their organs by using an RNA sequencing (RNA-seq)
117 analysis (Vu et al., 2019). We discovered that IR occurred even during this earlier stage
118 in the aging process when no change in protein level and no pathological changes in the
119 organs were observed and can thus be used as a new marker of the pre-disease state.
120 Detection of the pre-disease state is important for human health, because the state can
121 be reversible when it is appropriately treated. Here we provide definitive evidence that
122 JTT can specifically decrease the retained introns of genes for liver metabolic functions
123 among those that show an increase during the process of aging. With the support of both
124 transcriptome data related to differentially expressed genes (DEGs) and changes in the
125 metabolome, we suggest that JTT has a beneficial effect on metabolism in the liver at an
126 earlier stage of aging. We thus propose that the decrease in liver IR at this earlier stage
127 of aging by JTT is an indication of the effective actions of this herbal medicine at the
128 time corresponding to the pre-disease stage.
129
130 **Results**
131
132 **Looking for a marker of the pre-disease state in klotho mice at 7 weeks of age**
133
134 We used klotho mice, a model mouse for aging, for our experiment to look for a new
135 marker for the pre-disease state as well as a possible effect of a Japanese herbal
136 medicine on this state. Because aging is currently regarded as a kind of disease (see
137 Introduction), the pre-aging state can be regarded as a pre-disease state. We have chosen
138 the time of 7 weeks after birth for the date of sampling (Fig. 1AB), which is less than
139 half of the half-life of these mice (14.7 weeks; Fig. 1B). We expected that markers, if
140 any, isolated from these mice at 7 weeks would represent the pre-disease state. We also
141 designed our experiments to examine the effect of JTT on the improvement of the pre-
142 disease state (Fig. 1A). We designated klotho mice as KL and wild-type mice as WT,

143 each of which was fed with (+) or without (–) 0.5% JTT from 3.5 weeks of age until the
144 mice were 7 weeks old.
145 First, to examine the extent of aging of liver tissue in klotho mice, we looked for
146 histological changes at 7 weeks of age relative to liver tissue in WT mice. Fig. 1C
147 shows that there was no such alteration, indicating that the liver did not exhibit a
148 senescent phenotype at this age. Second, we chose several proteins and examined their
149 protein level by performing western blotting analysis (Fig. 1D). The representative
150 proteins are DDX5, SRSF6, and NXF1, all of which are splicing-related genes, and
151 PPARD and SIRT7, both of which are involved in metabolic pathways of the liver.
152 NDUFS2 is the core subunit of the mitochondrial Complex1, and LXRβ is encoded by
153 *Nr1h2* and regulates macrophage function. GAPDH was used as the loading control.
154 Furthermore, we checked the expression of RGN/SMP30, a marker of senescence
155 whose expression decreases with aging (Maruyama et al., 2010) (Fig. 1E). There was no
156 observable difference in the expression of these proteins between KL– and WT– (Fig.
157 1DE), and thus we can conclude that the klotho mouse liver at 7 weeks of age does not
158 show clear signs of aging.
159
160 **Metabolome analysis shows that klotho mice at 7 weeks of age express starvation-**
161 **like characteristics**
162
163 To look for possible internal changes in the liver that could describe the pre-disease
164 state in this earlier stage of aging, we investigated 110 metabolites of the liver using
165 CE-TOFMS (CE: capillary electrophoresis, TOFMS: time-of-flight mass spectrometry),
166 and compared metabolite levels between KL– and WT–, the comparison of which is a
167 measure of senescence. Among 12 metabolites that showed such differences, the data
168 for 7 metabolites ($P < 0.05$) are shown in Fig. 2. Remarkably, 3-hydroxybutyric acid (3-
169 HBA) was significantly increased in KL– (Fig. 2A), to a level 2.5 times higher than that
170 in WT–. 3-HBA is synthesized in the liver from fatty acid as one of the ketone bodies
171 under conditions of starvation and can be used as an energy source when blood glucose
172 is low (Fukao et al., 2014). Consistent with this, certain intermediate metabolites of
173 glycolysis, namely glucose 1-phosphate, fructose 1,6-diphosphate, dihydroxyacetone
174 phosphate, lactic acid, CoA divalent, and alanine in KL– were significantly decreased as
175 compared with their levels in WT– (Fig. 2B). These data suggest that klotho mice are
176 undergoing a fasting state, in spite of the presence of ample food, during which the
177 synthesis of 3-HBA is activated. Accordingly, an increase in 3-HBA and a reduction in
178 glycolysis in KL– might be representative of senescence in klotho mice.

179
180 **DEG analysis shows the alteration of gene expression during aging**
181
182 Knowing that the liver of klotho mice is under the starvation-like condition, we
183 performed RNA-seq analysis to look for a possible alteration of the gene expression
184 level in the liver during the pre-disease state. From liver collected from KL+, KL–,
185 WT+ and WT–, we isolated the mRNAs and then sequenced them. Multi-dimensional
186 scaling confirmed the consistency of each dataset (Fig. S1A). In addition,
187 transcriptomes from individual organs from KL+ and KL– indicated that JTT induced
188 extensive transcriptome changes (Fig. S1B).
189 We then extracted a down-regulated gene set and an up-regulated gene set in KL–
190 from the comparison of KL– and WT– (1228 genes and 1352 genes, respectively; Fig.
191 3A). The former represents genes whose expression decreased in the liver probably due
192 to aging-related deterioration, and the latter represents genes whose expression
193 increased possibly reflecting an adaptive response to aging. To characterize enriched
194 cell types in these genes, we performed a cell type enrichment (Cten) analysis
195 (Shoemaker et al., 2012) by using the software provided by these authors, in which, for
196 each cell type, a transcript was defined as a highly expressed cell-specific gene in that
197 cell if it had an expression value at least 15× greater than its median expression value
198 across all cells examined. The software can accurately identify the appropriate cell type
199 in a highly heterogeneous environment and provides insight into the suggested level of
200 enrichment to minimize the number of false discoveries. Fig. 3C shows that liver-
201 specific genes were especially enriched among the genes whose expression decreased
202 during aging, suggesting that liver function was reduced during aging. In contrast, a
203 variety of non-liver-specific cell types were enriched among those genes whose
204 expression increased during aging (Fig. 3D). It should be noted that several
205 macrophage-related cells were enriched in these increased genes, consistent with the
206 generally believed notion that the aging process activates innate immunity in spite of its
207 severe deterioration of adaptive immunity (Solana et al., 2006).
208
209 **DEG analysis shows the improvement in liver function as a result of JTT**
210 **administration**
211
212 To examine the influence of administration of JTT on the gene expression level in the
213 livers of klotho mice, we extracted the set of genes that were up-regulated and down-
214 regulated in KL+ after administration of JTT from the comparison of KL+ and KL–

215 (532 genes and 412 genes, respectively; Fig. 3B). Cten analysis of the up-regulated
216 genes demonstrated that liver-specific genes were highly enriched (Fig. 3E), whereas
217 that of down-regulated did not exhibit any enrich https://orcid.org/0000-0002-3655-
218 8060
219 ent. A comparison of the up-regulated gene set from the comparison of KL+ and KL–
220 (532 genes) and the down-regulated gene set in KL– from the comparison of KL– and
221 WT– (1228 genes) resulted in 213 DEGs, each of which exhibits the clear recovery
222 pattern from the decreased level of KL– to the level of WT– in the KL+ (Fig. 3F). Fig.
223 3G shows a boxplot summarizing the expression of 213 genes. Each data point was
224 normalized to the average expression level of each gene, and all the data were summed.
225 By using these genes, we performed a Cten analysis as shown in Fig. 3H and showed
226 that liver-specific functions are highly enriched in the 213 genes. We then extracted GO
227 terms enriched for these genes. Fig. 3I shows that genes related to liver-specific
228 functions, including metabolic process, flavonoid biosynthetic process, flavonoid
229 glucuronidation, and lipid metabolic process, were enriched, suggesting that the liver
230 functions were recovered by administration of JTT.
231
232 **IR and its recovery after administration of JTT is most prominent in the liver**
233
234 Knowing that klotho mice at 7 weeks of age represent a starvation-like state and that
235 their liver-specific functions at that time might be reduced due to the decreased
236 expression of liver-specific genes, we looked for possible changes in alternative splicing
237 at this age because it is known that several stresses can change alternative splicing
238 patterns (Boutz et al., 2015, Ninomiya et al., 2011, Shalgi et al., 2014; see later
239 discussion). We performed RNA-seq analysis in additional three organs, namely, blood,
240 kidney and heart for comparison.
241 To identify what type of alternative splicing is most prominent in the four organs
242 examined here, we first analyzed five types of alternative splicing, namely alternative 5'
243 splice site, alternative 3' splice site, skipped exon (SE), IR, and mutually exclusive
244 exons, between KL+ and KL– by using rMATS (Table 1-1). SE and IR were the most
245 prominent types of alternative splicing among the four organs. Noticeably, a change in
246 the frequency of IR in the liver was the most prominent effect followed by that in the
247 blood (Table 1-1).
248 We then calculated the difference in the frequency of IR in comparisons among
249 KL+, KL–, WT+, and WT– with the criteria of $P < 0.01$ (Table 1-2). We first noticed a
250 difference in the frequency of retained introns for the comparison between KL+ and

251 WT– was noted for only 59 loci, whereas that for KL– and WT– was noted for 212 loci.
252 The comparison between KL+ and WT– is a measure of the effect of JTT over
253 senescence, whereas the comparison between KL– and WT– measures the effect of the
254 senescence level in terms of the extent of retained introns accumulated during aging in
255 klotho mice. The above data suggest that the administration of JTT shifted the AS
256 pattern in klotho mice to be more similar to that of WT mice.
257 The 142 IR loci (Table 1-1 & -2) that were differentially affected between KL+ and
258 KL– in the liver included those genes for which the frequency of IR was decreased with
259 JTT in KL+ (132 loci; designated as "DecIR" type) and those genes for which the
260 frequency of IR was increased with JTT in KL+ (10 loci; designated as "IncIR" type)
261 (Fig. 4A). Likewise, the comparison between KL+ and KL– for the other three organs
262 showed a number of differential IR loci that could be divided into these two types. The
263 liver and blood exhibited higher values in the DecIR type as compared with the IncIR
264 type, whereas the other two organs, kidney and heart, had comparable values for DecIR
265 and IncIR (Fig. 4A). From these data, we designated liver and blood as two target
266 organs for JTT. Since we showed that the liver-specific function was recovered by
267 administration of JTT (see above), we focused in particular on the analyses of genes that
268 underwent a decrease in IR in the liver in response to JTT.
269
270 **Analysis of IR-recovered genes in the liver**
271
272 To demonstrate our strategy for evaluating the extent of IR, we first show an example
273 based on the data for *Anxa11* expression in the liver (Fig. 4C). *Anxa11* plays an
274 important role in cell division, $Ca^{2+}$ signaling, vesicle trafficking, and apoptosis (Han et
275 al., 2017). Sequenced *Anxa11* transcripts showed extensive accumulation of a retained
276 intron in KL–, whereas this intron was retained to a lesser extent for KL+ and WT–
277 (Fig. 4Ci).
278 Then, to analyze IR of *Anxa11* mathematically, we calculated the read counts of
279 skipping junctions (SJCs) and those of inclusion junctions (IJCs) for KL+, KL–, and
280 WT– (Fig. 4Cii) according to the strategy illustrated by rMATS (Fig. 4B). For KL+, we
281 then took the base-2 logarithm of the SJC/IJC ratio, which gives the fold change
282 (hereafter designated as FC) between the SJC and IJC at the intron junction (the thick
283 black bars in Fig. 4Ci). The same process was carried out for KL– and WT–, and the FC
284 values for KL+, KL–, and WT– were compared. The lower FC value for KL– was
285 recovered in KL+ to the same level as that of WT– (Fig. 4Ciii). The V shape of this bar

286 plot indicated a recovery from the senescence-type IR to the healthy-type IR after JTT
287 administration (see below).
288 As was described above, we first obtained the DecIR type (132 loci, 124 genes) in
289 klotho mice caused by JTT administration by comparing KL+ vs KL–. This simply
290 represents the recovery of retained introns in KL+. Then, we obtained the IncIR type
291 (190 loci, 180 genes) in klotho mice by comparing KL– vs WT–. This represents a
292 measure of the senescence-related changes in retained introns. Accordingly, the
293 comparison between these two types allowed us to highlight the effect of JTT at 7
294 weeks of age as shown in a Venn diagram (Fig. 5A). The overlapping 70 loci (67 genes)
295 represent the “complete recovery” loci, which are defined as those with significant
296 differences between KL+ and KL– and between KL– and WT–, but with FC values for
297 KL+ and WT– that were similar. The non-overlapping 62 (61 genes) and 120 loci (115
298 genes) represent "partial recovery" and "no recovery" loci, respectively. Fig. 5B shows a
299 heatmap of the 70 “complete recovery” loci, each of which represents a clear recovery
300 pattern. Fig. 5C is a boxplot of the FC values of KL+, KL–, and WT– for these 70 loci,
301 which shows the typical V-shaped pattern of recovery. Fig. 5D & E show boxplots of
302 the “partial recovery” loci and the “no recovery” loci, respectively. The former
303 represents loci with a significant difference between KL+ and KL– and without a
304 significant difference between KL– and WT–. The latter represents loci with a
305 significant difference between KL– and WT– and without a significant difference
306 between KL+ and KL–.
307
308 **Characteristics of loci with retained introns in the liver**
309
310 We next characterized introns among the 70 “complete recovery” loci, the 120 “no
311 recovery” loci and all other genes (~250,000 loci) expressed in the liver. The average
312 length of introns from the “complete recovery” and “no recovery” loci was significantly
313 shorter than that of all other introns (Fig. 6A). There was, however, no significant
314 difference in intron length between the “complete recovery” and “no recovery” loci,
315 suggesting that the “complete recovery” loci were not selectively discriminated from the
316 “no recovery” loci during the recovery process associated with JTT administration. The
317 GC content of introns associated with the “complete recovery” and “no recovery”
318 groups was significantly higher than that of all other liver-related introns (Fig. 6B).
319 Also, there was no significant difference between “complete recovery” and “no
320 recovery” introns in this respect, suggesting that GC content was not linked to recovery
321 status among IR loci. Then, we examined the strength of 5' and 3' splice sites by

322 calculating scores for these splice sites using the software MaxEntScan. The 5' splice
323 sites of introns of the “complete recovery” and “no recovery” loci were slightly but
324 significantly weaker than those of all other liver-related introns (Fig. 6C), but we found
325 no such differences at the 3' splice sites (Fig. 6D). These characteristics of introns at
326 IR loci were observed in the three additional organs (see below and Fig. S2A–D)
327 and are consistent with previous data (Braunschweig et al., 2014). Thus, loci with
328 shorter intron lengths, a higher GC content, and a weaker splicing score at the 5' site
329 have a tendency to have retained introns, but these are not characteristics that make
330 retained introns more likely to undergo recovery in the presence of JTT in the klotho
331 mice. We also confirmed the susceptibility of introns to IR in genes in terms of their
332 shorter intron length, higher GC content, and weaker intron score at the 5' splice site in
333 the other three organs (Fig. S2A–D) as was shown in the case of liver (Fig. 6).
334 Next, we searched for possible enrichment of binding sites for RNA-binding
335 proteins in the introns, as these are known to influence splice site selection and are
336 required for splicing (Padgett et al., 1986,Patel and Steitz, 2003). Binding sites for five
337 RNA-binding proteins were especially enriched in introns among the 70 “complete
338 recovery” loci but not among the 120 “no recovery” loci (Fig. 6E). This suggests that
339 genes expressed in the liver were more likely to recover from IR after JTT treatment if
340 they had these RNA-binding sites. Likewise, we examined the tendency for enrichment
341 for transcription factors (TFs) that bind to promoter regions in liver and in blood.
342 Binding sites for four TFs (Hoxa10, Hoxd12, Hoxd10, and Hoxd13) were especially
343 enriched in “complete recovery” genes in comparison with “no recovery genes” in liver
344 (Fig. 6F).
345
346 **Validation of IR-recovered genes in the liver by using RT-PCR**
347
348 Eleven genes were chosen for Integrative Genomics Viewer (IGV) mapping and RT-
349 PCR, which confirmed the recovery of IR upon JTT administration (Fig. 7, Fig. S3).
350 These genes are involved in RNA splicing (*Ddx5, Srsf5*) and typical liver functions such
351 as glucose and fatty acid metabolic pathways (*Sirt7*, *Acadm*, *Decr2*, *Gnmt*), lipid
352 metabolic processes (*Acadm*), heme biosynthesis and bile acid production (*Cyp27a1*,
353 *Hsd3b7*), and oxidation-reduction processes (*Acadm*, *Cyp27a1*, *Hsd3b7*).
354
355 **Biological function of IR-recovered genes in the liver**
356

357 Possible effects of JTT on the selection of liver retained intron loci for recovery during
358 aging were analyzed (Fig. 8). The results obtained from the Gene Ontology (GO)
359 analysis using Biological Process terms in Fig. 8A & B suggest two conclusions. First,
360 in the comparison between DecIR type (132 loci, 124 genes) of KL+ vs KL– and IncIR
361 type (190 loci, 180 genes) of KL– vs WT–, genes involved in RNA splicing and mRNA
362 processing are susceptible to IR during the aging process, and these retained introns
363 tend to be recovered by JTT (i.e., the red and blue bars are comparable; Fig. 8A). The
364 tendency of genes involved in these processes to be susceptible to IR during aging is
365 consistent with a previous study (Zane et al., 2014). These splicing-related genes can
366 control the expression of downstream genes through the regulation of their alternative
367 splicing. We defined 250 genes as potential splicing-related genes to highlight their
368 importance in the regulation of alternative splicing (see Methods for the definition of
369 splicing-related genes). They included almost all the spliceosomal proteins and
370 spliceosome regulatory proteins. Among 368 gene loci that exhibited a difference in
371 alternative splicing for the comparison of KL+ and KL– in the liver (Table 1-2), 19
372 genes (data not shown) were detected among the list of 250 potential splicing-related
373 genes. Among these 19 genes, 9 potential splicing-related genes in the liver were
374 subjected to IR, all of which exhibited the recovery pattern in terms of the comparison
375 in the FC among KL+, KL–, and WT– (Table 2). The patterns of recovery of the seven
376 potential splicing-related genes in liver associated with JTT administration together with
377 their FC values are shown in Fig. 7, Fig. 8D(i–iii), and Fig. S5B. Accordingly, JTT
378 appears to work in the direction of recovery, especially for potential splicing-related
379 genes.
380 Second, in addition to the recovery of IR for genes related to RNA splicing and
381 RNA processing, IR recovery was not evenly distributed among genes that accumulated
382 retained introns during aging but instead occurred selectively among liver-specific
383 genes. This conclusion was more obvious when loci of "complete recovery" (70 loci)
384 and "no recovery" (120 loci) were compared (Fig. 8B). The GO terms metabolic
385 process, oxidation-reduction process, carbohydrate metabolic process, and regulation of
386 gluconeogenesis, which represent major functions of the liver, were enriched among
387 genes that underwent "complete recovery" (i.e., red bars), whereas genes in the "no
388 recovery" group are associated with more general functions such as translation, protein
389 transport, and apoptosis (i.e., blue bars). These data suggest that, among genes
390 susceptible to IR during aging, the liver-specific genes selectively underwent a shift in
391 retained introns from the senescent state to the normal state after administration of JTT.

392 To further confirm that the recovery of retained introns by administration of JTT
393 occurred in liver-specific genes, Cten analysis was performed as shown in Fig. 8C.
394 Genes with "complete recovery" were significantly enriched among liver-specific genes
395 ($-\log_{10} P = 6.040$), confirming that the IR recovery from aging specifically occurred in
396 liver-specific genes.
397
398 **Biological function of IR-recovered genes in the blood**
399
400 To examine the characteristics of recovered genes among the other three organs, GO
401 analysis was performed for these organs, but only in the case of blood was the
402 significant enrichment of pathways with $P < 0.05$ observed (data not shown). GO
403 analysis for genes expressed in the blood that recovered from IR after JTT
404 administration indicated that the terms for immune system process and adaptive
405 immune response (Fig. S4B) were significantly enriched.
406
407 **Overlapping IR-recovered genes between liver and blood**
408
409 In addition to organ-specific genes with recovered IR, 11 genes that underwent IR
410 recovery were expressed in both the liver and blood (Fig. 8E, Fig. S5A). Fig. S5B
411 shows the patterns of IR recovery of genes that occurred in both of these organs.
412 Independent occurrence of recovery in different organs strongly suggests the
413 importance of the recovery of these genes for the organism. Among these 11 genes,
414 four splicing-related genes (*Sf3b1*, *Ddx5*, *Srsf5*, and *Srsf6*) were included, again
415 highlighting the importance of the recovery of these genes. Among the remaining
416 seven genes, we paid attention in particular to the following five genes, namely *Nr1h2*
417 (LXRβ), *Faah*, *Gdi1*, *Idh3g*, and *Sh3glb2* (EB2). *Nr1h2* is a key regulator gene in
418 macrophage function (Zelcer and Tontonoz, 2006). *Faah* is connected with
419 macrophage function through lipid metabolism (Xu et al., 2017), and *Gdi1* is
420 connected with interferon-γ activity through innate immunity (Ohshima et al.,
421 2015). *Idh3g* and *Sh3glb2* (EB2) are involved in mitochondrial function (Fino et al.,
422 2017). Considering that one of the prominent functions of JTT has been the activation
423 of the innate immune system, especially macrophage function, the recovery of IR
424 of *Nr1h2* (LXRβ), *Faah*, and *Gdi1* is especially interesting.
425
426 **Possible involvement of TFs in the increase in retained introns during aging and**
427 **their decrease by administration of JTT**

We first examined enrichment for TF-binding sites in the promoter region spanning 500 bp upstream from the transcription start site in the IR-increased genes in the liver (180 genes, 190 loci) and in the blood (12 genes, 12 loci), categorized as IncIR.KL– vs WT– (Fig. 9A). This type of data shows which TFs were possibly involved in the generation of retained introns that increased during progression of the pre-disease process. Most TFs were organ specific, as only two TFs, SPDEF and Sp1, were shared among genes in both organs, suggesting that they play a more general role in aging. We then examined enrichment for the binding sites of TFs in the IR-recovered genes in the liver (124 genes, 132 loci) and in the blood (39 genes, 40 loci), categorized as DecIR.KL+ vs KL– (Fig. 9B). These data clearly showed that different sets of TFs were used for transcription in IR-recovered genes in liver and in blood. Fig. 9C shows data from Fig. 9A & B for the liver, showing that some TFs were likely involved in both the increase and decrease of retained introns, whereas others were uniquely used in one case or the other.

This observation prompted us to examine how many IR-increased genes or IR-recovered genes in the respective organs have a common TF-binding site in the promoter region spanning 500 bp upstream from the transcription start site. In the case of an increase in IR during aging in the liver, 171 of 180 genes (190 loci) had at least one of four TFs, namely KLF14, SCL, THRb, and Zac1, as shown in Fig. 9D(i)(ii), which represents 95% coverage. In the case of a decrease in retained introns by administration of JTT, 120 of 124 genes (132 loci) had at least one of four TFs, namely SP2, Tgif2, KLF14, and Hoxd12, as shown in Fig. 9E(i)(ii), which represents 96.8% coverage. These data clearly show that a distinct set of genes sharing the same TF-binding sites was chosen during the IR-increasing process of aging and during the IR-decreasing process after administration of JTT and were networked. The significance of this observation will be discussed below.

A similar analysis was performed for the blood data, the results of which are shown in Fig. S6.

## Discussion

### IR is a marker of the pre-disease state

463 It has been proposed that retained intron accumulation is a signature for aging
464 (Adusumalli et al., 2019, Huan Li, 2017, Stegeman and Weake, 2017). In the present
465 study, we clearly demonstrated that IR occurs during the pre-disease state when neither
466 pathological alterations nor a difference in protein level could be observed. We
467 speculated that some disruption of homeostasis induced by a change in metabolites
468 triggered IR as a result of a stress during this earlier stage of aging. As shown in Fig.
469 2A, a significant increase in 3-HBA and decreases in intermediate metabolites of
470 glycolysis in KL– (Fig. 2B) suggest that the liver at this stage is subjected to starvation-
471 like conditions, providing the possibility that this starvation-like state is a stress signal
472 that triggers intron retention. Also, the decrease in 3-HBA in KL+, even if not
473 statistically significant, suggests at least a partial recovery from a starvation-like
474 condition. In addition, metabolome analysis also showed that the concentrations of
475 several nucleotides that are precursors of RNA were lower in KL– (Fig. 2C) relative to
476 that in WT–, suggesting that this also triggered intron retention. It is interesting to note
477 that the concentrations of some of these precursors recovered in KL+ to WT levels.
478 Accordingly, it is possible that the recovery of these precursors after the administration
479 of JTT affected the 180 IR-increased genes to reduce some of these retained introns to
480 the normal state, although this does not necessarily explain the reason why retained
481 introns of only a specific subset of genes were recovered to the normal state by JTT (see
482 the later discussion below).
483
484 **IR-recovered genes can be classified according to their functions**
485
486 Fig. 10A illustrates two major categories among the 132 IR-recovered genes, namely
487 alternative splicing and lipid/glucose metabolism. Splicing-related genes such as *Ddx5*,
488 *Sf3b1*, *Srsf5*, and *Srsf6* were included in these IR-recovered genes (Table 2). Splicing-
489 related genes are vulnerable to disruption of homeostasis in many systems, including
490 cancer (Dvinge and Bradley, 2015, Zhang and Manley, 2013), aging (Deschenes and
491 Chabot, 2017), and several stresses (Monteuuis et al., 2019, Shalgi et al., 2014). It is
492 possible that the IR recovery of some of these splicing-related genes reflects the
493 recovery of the normal splicing ability in KL+ after administration of JTT (see the later
494 discussion below).
495 In addition to genes involved in splicing, retained introns of genes involved in
496 lipid/glucose metabolism such as *Sirt7*, *Decr2*, *Acadm*, *Adipor1*, *Ppard*, *Nr1h2* (*LXRβ*),
497 and *Faah* were recovered (Fig. 10A). They are relevant to hepatic metabolic pathways
498 involving glucose and fatty acids. Under fasting or starvation conditions, endogenous

499 glucose is mainly produced by a breakdown of glycogen and gluconeogenesis in the
500 liver and is metabolized into pyruvate, which is used to generate ATP through the
501 tricarboxylic acid cycle and oxidative phosphorylation in mitochondria (Nishi et al.,
502 2017). In addition, fatty acids are oxidized through hepatic mitochondrial β-oxidation to
503 generate ketone bodies. Thus, liver-produced glucose and ketone bodies provide
504 essential sources of energy for extrahepatic tissues during fasting and starvation (Rui,
505 2014). Metabolome analysis showed that the condition of the liver in KL– resembled
506 starvation and that the condition of the liver in KL+ was improved, suggesting that the
507 improvement in the condition of KL+ triggered a cue for the recovery of IR of these
508 genes (see the model proposed below).
509 In addition to genes belonging to these two categories, a few genes involving
510 mitochondrial processes and immune system and macrophage processes are also
511 included in these IR-recovered genes. These are listed and referenced in the legend of
512 Fig. 10A, in which the possibility is discussed that the IR recovery of several nuclear
513 receptor genes such as *Nr1h2* (LXRβ) might reflect the effect of JTT on macrophage
514 function.
515
516 **Some liver metabolic functions were improved to the normal state by**
517 **administration of JTT**
518
519 Before discussing a model concerning the mechanism by which only certain genes
520 undergo IR recovery in response to JTT, we highlight the results of 213 genes from the
521 DEG analysis, the expression levels of which were down-regulated in KL– and were
522 recovered to the level of WT– in KL+ (Fig.3G). GO analysis of these genes showed that
523 metabolic processes and glucuronidation in the liver likely were up-regulated in KL+
524 and had recovered after administration of JTT from the down-regulated state in KL–
525 (Fig. 3I).
526 There are many clinical and basic scientific reports on the improvement of liver
527 functions by JTT, typically exemplified by reports that JTT can protect the liver from
528 injury by chemicals administered to patients with cancer or other diseases. A few
529 examples are listed below (others are listed in the legend for Fig. 10A). JTT protects
530 against isoniazid/rifampicin-induced hepatic injury by modulating oxidative stress and
531 inflammatory responses (Yoshioka et al., 2019). JTT exerts protective effects against
532 alcohol-induced liver disease by modulating oxidative stress and the inflammatory
533 response (Fukaya et al., 2018). JTT has the potential to protect against bromobenzene-
534 induced hepatotoxicity and to modulate oxidative stress (Yoshioka et al., 2016). The

535 presence of such a variety of reports convinced us that an improvement in liver
536 function, especially metabolic activities, is one of the major effects of JTT. These
537 published data are consistent with our DEG data described above.
538
539 **A model to explain the reason why IR in a specific subset of genes involving liver**
540 **metabolism was recovered**
541
542 As was mentioned in the Introduction, IR has been considered to be harmful to the
543 organism (Weischenfeldt et al., 2005). Recent global screens across many cells and
544 tissue types from humans and mice, however, have gradually revealed the role of IR as
545 a negative regulator of gene expression that is integrated into a regulatory network of
546 RNA processing and has functional significance (Braunschweig et al., 2014, Jacob and
547 Smith, 2017, Liu et al., 2017). Recent studies have shown that programmed IR is a
548 critical regulatory pathway in normal development and differentiation, such as in
549 granulocyte differentiation (Wong et al., 2013), terminal erythroid differentiation
550 (Pimentel et al., 2016), male germ cell differentiation (Naro et al., 2017) and B cell
551 development (Ullrich & Guigo, 2019). The fact that IR within the cyclin A2 gene
552 induces G1/S arrest in differentiated human tissues suggests that IR may play a role in
553 cell differentiation and senescence through regulation of the cell cycle (Honda et al.,
554 2012).
555 During the heat shock response in mice, there is widespread retention of introns in
556 transcripts from 1,700 genes, which are enriched for tRNA synthetase, nuclear pore, and
557 spliceosome functions. These transcripts with retained introns are, for the most part,
558 nuclear and untranslated. These splicing-inhibited transcripts induced by heat shock
559 stress are mostly spliced post-transcriptionally, in contrast to other normal splicing that
560 occurs co-transcriptionally (Shalgi et al., 2014). These nuclear retained transcripts are
561 presumed to await a signal for splicing that is cued by the release from the stress (Jacob
562 and Smith, 2017). The presence of other similar examples (Boutz et al., 2015, Ninomiya
563 et al., 2011) of stress-induced regulation of intron retention suggests that this regulatory
564 mechanism contributes to a wide range of gene expression.
565 As aging is also a kind of stress, we considered intron retention during aging as
566 analogous to that which occurs during the heat shock response as described above. Fig.
567 10C(i) shows a model for the case of KL– in that transcripts with IR are retained in the
568 nucleus upon the stress signal of aging such that global metabolic activity in liver cells
569 is repressed to save energy. After administration of JTT, as liver-specific metabolic
570 functions are recovered to some extent as described above, improvement in metabolic

571 activity results in a signal to the liver cells to recover these retained introns by sending a
572 cue for post-transcriptional splicing (Fig. 10C(ii)). If this model is correct, we can
573 determine which pathways in the cells are improved by knowing which functions the
574 IR-recovered genes are involved in. In the present case, the recovery of retained introns
575 of genes involved in lipid/glucose metabolic pathways (Fig. 10A) suggests that the
576 liver-specific metabolic functions were recovered. Genes detected by DEG data (Fig. 3F
577 G), the Cten analysis (Fig. 3H), and its GO analysis (Fig. 3I) confirmed that this is the
578 case. Also, the recovery of retained introns of genes involved in splicing pathways (Fig.
579 8A) suggests that splicing functions were recovered, at least in part. In addition, since a
580 few genes involving mitochondrial processes and immune system and macrophage
581 processes are also included in the IR-recovered genes, we speculate that these functions
582 were also recovered by administration of JTT.
583
584 **The mechanism for aging-related intron retention in transcripts and possible gene**
585 **specificity of JTT-related recovery**
586
587 Regarding the mechanisms related to how transcripts retained their introns and to
588 how a specific group of transcripts was recovered, we suggested above that IR-
589 susceptible genes during aging and IR-recovered genes after JTT administration are
590 transcriptionally controlled by a very few TFs that are specific to the liver and blood
591 (Fig. 9). There is emerging evidence that mRNA splicing is controlled by multi-layered
592 mechanisms that involve transcription and epigenetics (Braunschweig et al., 2014, Lev
593 Maor et al., 2015, Luco et al., 2011). Therefore, it is possible that TFs, chromatin
594 constituents, and epigenetic factors such as those related to histone modification and
595 DNA methylation not only control transcription but also regulate splicing (Lev Maor et
596 al., 2015, Luco et al., 2011). These factors can affect the rate of RNA polymerase II
597 elongation, which in turn affects the pattern of alternative splicing. Accordingly, it is
598 possible that accumulation of retained introns during aging in klotho mice was caused
599 by a change in the elongation rate of transcription. As shown in Fig. 9, there are several
600 TF-binding sites that are enriched in the IR-susceptible genes during aging (190 loci,
601 180 genes). Accordingly, an aging signal such as fasting may lead specific TFs to retard
602 the transcription rate, resulting in IR. Also, it is possible that some active ingredients of
603 JTT in cooperation with these TFs could contribute to the recovery of IR.
604 Also, it is interesting to note that the concentration of certain nucleotide diphosphates
605 (UDP and GDP) was decreased in KL– and recovered to WT levels in KL+ (Fig. 3C). If
606 a low concentration of nucleotides triggers a change in the elongation rate of

607 transcription (Kwak and Lis, 2013), it is also possible that this may have induced the
608 accumulation of retained introns. The recovery of such concentrations to the normal
609 level in KL+ is consistent with the recovery of retained introns in KL+.
610 Although there are instances in which chemical compounds influence AS by directly
611 interacting with splicing factors (Kataoka, 2017), there has been no report of changes in
612 AS patterns that result from an interaction with a TF. It is of interest to examine whether
613 active ingredients of a Kampo medicine can interact with TFs to influence AS patterns
614 co-transcriptionally or post-transcriptionally. The current results regarding the reduction
615 of retained introns by JTT will provide a rich resource for the subsequent studies of the
616 regulation of AS.
617
618 **Perspective**
619
620 This study is the first to shed light on the comprehensive mechanism of a multi-herbal
621 medicine from the viewpoint of systems biology. It is interesting to note that the ancient
622 Chinese medical textbook *Inner Canon of the Yellow Emperor* stated that the pre-
623 disease state should be treated early with Kampo medicine (UNESCO, 2011). The
624 present data represent a molecular proof of this historical statement. Kampo medicine is
625 a precious heritage in Japan, and there are similar medicines used around the world such
626 as traditional Chinese medicines (Patwardhan et al., 2005), traditional medicines in
627 India (Ayurveda) (Patwardhan et al., 2005), and ancient Greek medicines (Unani
628 medicine). To elucidate the mechanisms of these medicines, which are the result of
629 human wisdom that has accumulated over several thousand years, and to pass on this
630 knowledge to subsequent generations are the main goals of our research.
631
632 **Materials and Methods**
633
634 **Juzen-taiho-to (JTT)**
635
636 JTT was supplied by Tsumura & Co. (Tokyo, Japan) in the form of a powdered
637 extract. It was obtained by spray-drying a hot water extract mixture of the following 10
638 crude drugs in the ratios provided in parentheses: Astragali radix (10.52), Cinnamomi
639 cortex (10.52), Rehmanniae radix (10.52), Paeoniae radix (10.52), Cnidii rhizome
640 (10.52), Atractylodis lanceae rhizome (10.52), Angelicae radix (10.52), Ginseng radix
641 (10.52), Poria (10.52), and Glycyrrhizae radix (5.32). The origins and species of each
642 component, the contents of characteristic ingredients, and other pharmaceutical-grade

643 qualities of JTT are strictly controlled as it is an ethical drug approved by the Ministry
644 of Health, Welfare and Labor of Japan.
645
646 **RNA extraction and RNA-seq**
647
648 After removal of organs, they were subjected to RNA extraction after being soaked
649 with RNALater (Thermo Fisher Scientific, Rockford, IL, USA). RNA extraction was
650 performed on individual tissue samples with the Pure Link RNA Mini kit (Invitrogen,
651 MA, USA). Briefly, 600 μL of Lysis Buffer and 900 μL of TRIzol (Thermo Fisher
652 Scientific) were added to 0.03 g of tissue, and the tissue was homogenized. After the
653 sample was incubated for 10 min at room temperature and centrifuged at 12,000 × *g* for
654 15 min, the supernatant was treated with DNase and purified by column cartridge. The
655 quality of RNA was checked by Qubit (Thermo Fisher Scientific) and TapeStation
656 (Agilent Technologies, CA, USA). RNA library construction was performed by using a
657 TruSeq Stranded mRNA Sample Prep kit (Illumina, CA, USA). Paired-end (150 base
658 pairs × 2) sequencing with the NovaSeq 6000 platform (Illumina) was outsourced to
659 Takara Bio, Shiga, Japan.
660
661 **Quality check and filtering of RNA-seq data and mapping analysis**
662
663 For purification of the sequencing data, cutadapt v.1.16 (Deschenes and Chabot, 2017)
664 was used to remove Illumina adapter sequences, followed by removal of the poly(A)
665 sequence using fastx_clipper software in the fastx toolkit software package v.0.0.14
666 (http://hannonlab.cshl.edu/fastx_toolkit/). To remove low-quality bases or sequences,
667 we trimmed the sequences using fastq_quality_trimmer software (parameters: -t 20 -l 30
668 -Q 33) and fastq_quality_filter software (parameters: -q 20 -p 80 -Q 33), both of which
669 are included in the fastx toolkit. During the above processing, any read in which one of
670 the pairs was missing was removed using Trimmomatic v.0.38 (Bolger et al., 2014).
671 Then, reads containing mouse rRNA, tRNA, or phiX sequences as the control sequence
672 from Illumina were removed using Bowtie 2 v. 2.3.4.1 (Langmead and Salzberg, 2012).
673 We then carried out the second round of removal of any unpaired reads using
674 bam2fastq. After completion of these filtering steps, 20 million reads of each of the
675 forward and reverse sequences per sample were mapped to the mouse genome sequence
676 build GRCm38 using Tophat v2.1.1 (Trapnell et al., 2009). The mouse genome
677 sequence was downloaded from iGenomes of Illumina
678 (http://jp.support.illumina.com/sequencing/sequencing_software/igenome.html).

679 Multiple mapped reads were removed using samtools (parameters: samtools view -q 4).
680 Uniquely mapped reads were counted by gene annotation (Ensembl release 81) using
681 featureCounts v.1.6.2. The counted values were normalized with the TMM method
682 using EdgeR library in R v.3.5.0 and used for expression analysis.
683
684 **Analysis of alternative splicing**
685
686 Loci with significantly different splicing patterns with $P < 0.01$ were detected within
687 six combinations: KL+/KL–, KL+/WT+, KL+/WT–, KL–/WT+, KL–/WT–, and
688 WT+/WT–, where '+' and '–' refer to treatment with and without, respectively, JTT,
689 using rMATS v.4.0.2 (Shen et al., 2014). Statistical significance was tested using the
690 skipping junction counts (SJCs) and the inclusion junction counts (IJCs) as calculated
691 by rMATS at the corresponding loci. We checked the mapping status and generated the
692 mapping result view using IGV (http://software.broadinstitute.org/software/igv/)
693 (Robinson et al., 2011).
694
695 **Analysis of characteristics for the IR gene group**
696
697 We analyzed enriched gene functions and pathways at 142 loci (134 genes) at which
698 significantly different IR events were detected between KL+ and KL– using DAVID ver
699 6.8 (https://david.ncifcrf.gov/) (Huang da et al., 2009) with the following criteria: Count
700 ≥ 1, EASE ≤ 1.
701
702 **Splice site score**
703
704 For the evaluation of splice site strength, maximum entropy scores for 5' and 3' splice
705 sites were calculated using MaxEntScan (Yeo and Burge, 2004).
706
707 **Motif analysis**
708
709 For the comparison of protein-binding motifs in the mRNA, we compared motifs with
710 the ATtRACT database of RNA-biding proteins and their associated motifs (Giudice et
711 al., 2016). We compared TF-binding sites using HOMER (Heinz et al., 2010) with
712 default parameters. All detected motifs were then compared using Fisher's test.
713
714 **Definition of potential splicing-related genes**

715
716 The KEGG pathway lists ~140 proteins as spliceosomal proteins, and we then added
717 109 genes from the Gene Ontology (GO) list (GO:0000398) of mRNA splicing via
718 spliceosome. We also added 66 genes from the GO list (GO:0003729) of mRNA
719 binding and 180 genes from the GO list (GO:0006397) of mRNA processing, both of
720 which were chosen to overlap with genes listed by Han et al. (2017) that were selected
721 based on the criterion that a knock-down experiment influenced their alternative
722 splicing. After removing duplicates, we ultimately defined 250 genes as potential
723 splicing-related genes in this analysis. They included almost all the spliceosomal
724 proteins and spliceosome regulatory proteins.
725
726 **Reverse transcription PCR amplification of IR loci**
727
728 The extracted RNA was treated with Recombinant DNase I (Takara Bio, Japan) to
729 digest the remaining genomic DNA and was purified by phenol/chloroform/isoamyl
730 alcohol (25:24:21) and ethanol precipitation. The purified RNA was reverse transcribed
731 using High-Capacity cDNA Reverse Transcription kits (Thermo Fisher Scientific).
732 Primers were prepared in exons adjacent to the IR locus, and PCR amplification was
733 performed using the cDNA. Reaction conditions were as follows: 5 μL 10× PCR buffer
734 (Takara Bio), 5 μL dNTPs (25 mM; Takara Bio), 1 μL primers (10 pmol/μL each
735 primer), 0.2 μL ExTaq DNA polymerase (5 U/μL; Takara Bio), 40 ng of template DNA,
736 and DNase-free water added to a final volume of 50 μL. PCR was performed using
737 GeneAmp PCR system 9700 (Thermo Fisher Scientific) with the following conditions:
738 initial annealing at 96°C for 5 min, followed by 25 or 30 cycles (96ºC for 30 sec, 55ºC
739 for 45 sec, 72ºC for 2 min). After a final extension at 72°C for 5 min, the PCR mixtures
740 were held at 4°C. The amplicon was confirmed based on size by TapeStation. The
741 primer set used is listed in supplementary information (SI). Primer sequences were
742 listed in Table S1.
743
744 **Analysis of DEG**
745
746 Genes that had significantly differential expression with $P < 0.01$ in two comparisons,
747 namely KL+/KL– and KL–/WT–, were detected using edgeR (Robinson et al., 2010).
748 The recovered genes that were significantly down-regulated in KL– as compared with
749 WT– and significantly up-regulated in KL+ as compared with KL– were extracted.
750

751 **Western blot analysis**
752
753 Mouse liver samples were homogenized in ice-cold RIPA buffer (50 mM Tris, 150 mM
754 NaCl, 1% NP-40, 0.5% deoxycholic acid sodium monohydrate, 0.1% SDS, 10 mM
755 NaF, pH 7.4) with a Disposable homogenizer (Nippi BioMasher) (30 strokes), and the
756 homogenates were centrifuged at 10,000 × *g* and 4°C for 20 min. The protein
757 concentration of each supernatant was measured by the BCA protein assay (Thermo
758 Fisher Scientific), and supernatants were diluted to equal protein concentrations,
759 combined with 2 M DTT (final concentration, 0.2 M) and 4× SDS sample buffer (6%
760 SDS, 40% glycerol, 0.4% bromophenol blue, 250 mM Tris, pH 6.8), and boiled for 5
761 min at 95°C.
762 Protein samples (30 μg/well) were resolved by SDS-PAGE and then transferred onto
763 PVDF membranes. The membranes were blocked with 5% milk in TBST (20 mM Tris,
764 150 mM NaCl, containing 0.05% Tween-20, pH 7.4) and incubated with primary
765 antibodies at 4°C overnight. Primary antibodies used in this study were anti-
766 RGN/SMP30 (17947-1-AP, Proteintech), anti-DDX5,p68 (10804-1-AP, Proteintech),
767 anti-NDUFS2 (GTX114924, GeneTex), anti-PPARD (10156-2-AP, Proteintech), anti-
768 SIRT7 (12994-1-AP, Proteintech), anti-NXF1 (10328-1-AP, Proteintech), anti-SRSF6
769 (11772-1-AP, Proteintech), anti-LXR beta (ab28479, Abcam), and anti-GAPDH (sc-
770 32233, Santa Cruz Biotechnology). After incubation with secondary antibodies
771 peroxidase-conjugated anti–rabbit IgG (SA00001-2, Proteintech) or anti–mouse IgG
772 (sc-516102, Santa Cruz Biotechnology), protein bands were detected using ECL Prime
773 Western Blotting Detection Reagents (GE Healthcare). Some of the membranes were
774 probed with anti-GAPDH , which was used as the loading control for other blots in each
775 experiment. The signal intensity was quantified using ImageJ (NIH) or a ChemiDoc
776 system (Bio-Rad). Western blots were repeated a minimum of three times with different
777 animals, and representative blots are shown.
778
779 **Data availability**
780
781 The original RNA-seq datasets have been deposited in the DDBJ Sequence Read
782 Archive under accession numbers DRR167982–DRR167990, which are linked to the
783 BioProject accession number PRJDB7898.
784
785 **Acknowledgements**
786

The present work was financially supported by FAIS and Zenick Co. represented by Mr. Y. Otake and Mr. T. Sugino, respectively. We thank Mr. K. Onodera for management and discussions and Ms. A. Koizumi for making illustrations.

**Competing interests**

N.O., K.O., Y.I., A.M., E.I., T.V., and S.N., received a research grant from Zenick Co. and Tsumura & Co. N.F., A.N., A.S., M.N., A.K., and M.Y. are employees of Tsumura & Co.

**References**

1. Adusumalli, S., Ngian, Z.K., Lin, W.Q., Benoukraf, T., and Ong, C.T. (2019). Increased intron retention is a post-transcriptional signature associated with progressive aging and Alzheimer's disease. *Aging Cell* **18**(3), e12928. DOI: 10.1111/acel.12928.
2. Bolger, A.M., Lohse, M., and Usadel, B. (2014). Trimmomatic: a flexible trimmer for Illumina sequence data. *Bioinformatics* **30**(15), 2114-2120. DOI: 10.1093/bioinformatics/btu170.
3. Boutz, P.L., Bhutkar, A., and Sharp, P.A. (2015). Detained introns are a novel, widespread class of post-transcriptionally spliced introns. *Genes Dev* **29**(1), 63-80. DOI: 10.1101/gad.247361.114.
4. Braunschweig, U., Barbosa-Morais, N.L., Pan, Q., Nachman, E.N., Alipanahi, B., Gonatopoulos-Pournatzis, T., Frey, B., Irimia, M., and Blencowe, B.J. (2014). Widespread intron retention in mammals functionally tunes transcriptomes. *Genome Res* **24**(11), 1774-1786. DOI: 10.1101/gr.177790.114.
5. Deschenes, M., and Chabot, B. (2017). The emerging role of alternative splicing in senescence and aging. *Aging Cell* **16**(5), 918-933. DOI: 10.1111/acel.12646.
6. Dvinge, H., and Bradley, R.K. (2015). Widespread intron retention diversifies most cancer transcriptomes. *Genome Med* **7**(1), 45. DOI: 10.1186/s13073-015-0168-9.
7. Dvinge, H., Kim, E., Abdel-Wahab, O., and Bradley, R.K. (2016). RNA splicing factors as oncoproteins and tumour suppressors. *Nat Rev Cancer* **16**(7), 413-430. DOI: 10.1038/nrc.2016.51.

8. Fino, K.K., Yang, L., Silveyra, P., Hu, S., Umstead, T.M., DiAngelo, S., Halstead, E.S., Cooper, T.K., Abraham, T., Takahashi, Y., *et al.* (2017). SH3GLB2/endophilin B2 regulates lung homeostasis and recovery from severe influenza A virus infection. *Scientific Reports* **7**(1), 7262. DOI: 10.1038/s41598-017-07724-5.

9. Fouache, A., Zabaiou, N., De Joussineau, C., Morel, L., Silvente-Poirot, S., Namsi, A., Lizard, G., Poirot, M., Makishima, M., Baron, S., *et al.* (2019). Flavonoids differentially modulate liver X receptors activity-Structure-function relationship analysis. *J Steroid Biochem Mol Biol* **190**, 173-182. DOI: 10.1016/j.jsbmb.2019.03.028.

10. Fukao, T., Mitchell, G., Sass, J.O., Hori, T., Orii, K., and Aoyama, Y. (2014). Ketone body metabolism and its defects. *J Inherit Metab Dis* **37**(4), 541-551. DOI: 10.1007/s10545-014-9704-9.

11. Fukaya, S., Nagatsu, A., and Yoshioka, H. (2018). The Kampo formula "Juzen-taiho-to" exerts protective effects on ethanol -induced liver injury mice. *Fundamental Toxicological Sciences* **5**(3), 105-112. DOI: doi:10.2131/fts.5.105

12. Giudice, G., Sanchez-Cabo, F., Torroja, C., and Lara-Pezzi, E. (2016). ATtRACT-a database of RNA-binding proteins and associated motifs. *Database (Oxford)* **2016**. DOI: 10.1093/database/baw035.

13. Han, H., Braunschweig, U., Gonatopoulos-Pournatzis, T., Weatheritt, R.J., Hirsch, C.L., Ha, K.C.H., Radovani, E., Nabeel-Shah, S., Sterne-Weiler, T., Wang, J., *et al.* (2017). Multilayered Control of Alternative Splicing Regulatory Networks by Transcription Factors. *Mol Cell* **65**(3), 539-553 e537. DOI: 10.1016/j.molcel.2017.01.011.

14. Heinz, S., Benner, C., Spann, N., Bertolino, E., Lin, Y.C., Laslo, P., Cheng, J.X., Murre, C., Singh, H., and Glass, C.K. (2010). Simple combinations of lineage-determining transcription factors prime cis-regulatory elements required for macrophage and B cell identities. *Mol Cell* **38**(4), 576-589. DOI: 10.1016/j.molcel.2010.05.004.

15. Honda, A., Valogne, Y., Bou Nader, M., Brechot, C., and Faivre, J. (2012). An intron-retaining splice variant of human cyclin A2, expressed in adult differentiated tissues, induces a G1/S cell cycle arrest in vitro. *PLoS One* **7**(6), e39249. DOI: 10.1371/journal.pone.0039249.

16. Huan Li, Z.W., Tianyi Ma, Gang Wei, Ting Ni (2017). Alternative splicing in aging and age-related diseases. *Translational Medicine of Aging* **1**, 32-40. DOI, https://www.sciencedirect.com/science/article/pii/S246850111730007X.

859 17. Huang da, W., Sherman, B.T., and Lempicki, R.A. (2009). Systematic and
860 integrative analysis of large gene lists using DAVID bioinformatics resources. *Nat*
861 *Protoc* **4**(1), 44-57. DOI: 10.1038/nprot.2008.211.
862 18. Ishikawa, S., Ishikawa, T., Tezuka, C., Asano, K., Sunagawa, M., and Hisamitsu,
863 T. (2017). Efficacy of Juzentaihoto for Tumor Immunotherapy in B16 Melanoma
864 Metastasis Model. *Evid Based Complement Alternat Med* **2017**, 6054706. DOI:
865 10.1155/2017/6054706.
866 19. Jacob, A.G., and Smith, C.W.J. (2017). Intron retention as a component of
867 regulated gene expression programs. *Hum Genet* **136**(9), 1043-1057. DOI:
868 10.1007/s00439-017-1791-x.
869 20. Kaneko, A., Matsumoto, T., Matsubara, Y., Sekiguchi, K., Koseki, J., Yakabe, R.,
870 Aoki, K., Aiba, S., and Yamasaki, K. (2017). Glucuronides of phytoestrogen
871 flavonoid enhance macrophage function via conversion to aglycones by beta-
872 glucuronidase in macrophages. *Immun Inflamm Dis* **5**(3), 265-279. DOI:
873 10.1002/iid3.163.
874 21. Kataoka, N. (2017). Modulation of aberrant splicing in human RNA diseases by
875 chemical compounds. *Hum Genet* **136**(9), 1237-1245. DOI: 10.1007/s00439-017-
876 1789-4.
877 22. Kitamura, K., Iino, Y., Kamide, Y., Kudo, F., Nakayama, T., Suzuki, K., Taiji, H.,
878 Takahashi, H., Yamanaka, N., and Uno, Y. (2015). Clinical practice guidelines for
879 the diagnosis and management of acute otitis media (AOM) in children in Japan -
880 2013 update. *Auris Nasus Larynx* **42**(2), 99-106. DOI: 10.1016/j.anl.2014.09.006.
881 23. Ko, J.H., Lee, J.H., Choi, B., Park, J.Y., Kwon, Y.W., Jeon, S., Park, S.D., and Kim,
882 S.N. (2018). Neuroprotective Effects of Gagam-Sipjeondaebo-Tang, a Novel
883 Herbal Formula, against MPTP-Induced Parkinsonian Mice and MPP(+)-Induced
884 Cell Death in SH-SY5Y Cells. *Evid Based Complement Alternat Med* **2018**,
885 2420809. DOI: 10.1155/2018/2420809.
886 24. Kuro-o, M., Matsumura, Y., Aizawa, H., Kawaguchi, H., Suga, T., Utsugi, T.,
887 Ohyama, Y., Kurabayashi, M., Kaname, T., Kume, E., *et al.* (1997). Mutation of
888 the mouse klotho gene leads to a syndrome resembling ageing. *Nature* **390**(6655),
889 45-51. DOI: 10.1038/36285.
890 25. Kwak, H., and Lis, J.T. (2013). Control of transcriptional elongation. *Annu Rev*
891 *Genet* **47**, 483-508. DOI: 10.1146/annurev-genet-110711-155440.
892 26. Langmead, B., and Salzberg, S.L. (2012). Fast gapped-read alignment with Bowtie
893 2. *Nat Methods* **9**(4), 357-359. DOI: 10.1038/nmeth.1923.
894 27. Lejeune, F., and Maquat, L.E. (2005). Mechanistic links between nonsense-

895 mediated mRNA decay and pre-mRNA splicing in mammalian cells. *Curr Opin*
896 *Cell Biol* **17**(3), 309-315. DOI: 10.1016/j.ceb.2005.03.002.
897 28. Lev Maor, G., Yearim, A., and Ast, G. (2015). The alternative role of DNA
898 methylation in splicing regulation. *Trends Genet* **31**(5), 274-280. DOI:
899 10.1016/j.tig.2015.03.002.
900 29. Liu, Y., Gonzalez-Porta, M., Santos, S., Brazma, A., Marioni, J.C., Aebersold, R.,
901 Venkitaraman, A.R., and Wickramasinghe, V.O. (2017). Impact of Alternative
902 Splicing on the Human Proteome. *Cell Rep* **20**(5), 1229-1241. DOI:
903 10.1016/j.celrep.2017.07.025.
904 30. Lopez-Otin, C., Blasco, M.A., Partridge, L., Serrano, M., and Kroemer, G. (2013).
905 The hallmarks of aging. *Cell* **153**(6), 1194-1217. DOI: 10.1016/j.cell.2013.05.039.
906 31. Luco, R.F., Allo, M., Schor, I.E., Kornblihtt, A.R., and Misteli, T. (2011).
907 Epigenetics in alternative pre-mRNA splicing. *Cell* **144**(1), 16-26. DOI:
908 10.1016/j.cell.2010.11.056.
909 32. Maruyama, N., Ishigami, A., and Kondo, Y. (2010). Pathophysiological
910 significance of senescence marker protein-30. *Geriatr Gerontol Int* **10 Suppl 1**,
911 S88-98. DOI: 10.1111/j.1447-0594.2010.00586.x.
912 33. Matsumoto, T., Sakurai, M.H., Kiyohara, H., and Yamada, H. (2000). Orally
913 administered decoction of Kampo (Japanese herbal) medicine, "Juzen-Taiho-To"
914 modulates cytokine secretion and induces NKT cells in mouse liver.
915 *Immunopharmacology* **46**(2), 149-161. DOI: 10.1016/S0162-3109(99)00166-6.
916 34. Mayeda, A., Munroe, S.H., Caceres, J.F., and Krainer, A.R. (1994). Function of
917 conserved domains of hnRNP A1 and other hnRNP A/B proteins. *EMBO J* **13**(22),
918 5483-5495. DOI: 10.1002/j.1460-2075.1994.tb06883.x
919 35. Monteuuis, G., Wong, J.J.L., Bailey, C.G., Schmitz, U., and Rasko, J.E.J. (2019).
920 The changing paradigm of intron retention: regulation, ramifications and recipes.
921 *Nucleic Acids Res* **47**(22), 11497-11513. DOI: 10.1093/nar/gkz1068.
922 36. Munakata, K., Takashima, K., Nishiyama, M., Asano, N., Mase, A., Hioki, K.,
923 Ohnishi, Y., Yamamoto, M., and Watanabe, K. (2012). Microarray analysis on
924 germfree mice elucidates the primary target of a traditional Japanese medicine
925 juzentaihoto: acceleration of IFN-alpha response via affecting the ISGF3-IRF7
926 signaling cascade. *BMC Genomics* **13**, 30. DOI: 10.1186/1471-2164-13-30.
927 37. Naro, C., Jolly, A., Di Persio, S., Bielli, P., Setterblad, N., Alberdi, A.J., Vicini, E.,
928 Geremia, R., De la Grange, P., and Sette, C. (2017). An Orchestrated Intron
929 Retention Program in Meiosis Controls Timely Usage of Transcripts during Germ
930 Cell Differentiation. *Dev Cell* **41**(1), 82-93 e84. DOI:

931 10.1016/j.devcel.2017.03.003.
932 38. Niemela, E.H., Oghabian, A., Staals, R.H., Greco, D., Pruijn, G.J., and Frilander,
933 M.J. (2014). Global analysis of the nuclear processing of transcripts with
934 unspliced U12-type introns by the exosome. *Nucleic Acids Res* **42**(11), 7358-7369.
935 DOI: 10.1093/nar/gku391.
936 39. Ninomiya, K., Kataoka, N., and Hagiwara, M. (2011). Stress-responsive
937 maturation of Clk1/4 pre-mRNAs promotes phosphorylation of SR splicing factor.
938 *J Cell Biol* **195**(1), 27-40. DOI: 10.1083/jcb.201107093.
939 40. Nishi, A., Ohbuchi, K., Kushida, H., Matsumoto, T., Lee, K., Kuroki, H.,
940 Nabeshima, S., Shimobori, C., Komokata, N., Kanno, H., *et al.* (2017).
941 Deconstructing the traditional Japanese medicine "Kampo": compounds,
942 metabolites and pharmacological profile of maoto, a remedy for flu-like
943 symptoms. *NPJ Syst Biol Appl* **3**, 32. DOI: 10.1038/s41540-017-0032-1.
944 41. Ohshima, J., Sasai, M., Liu, J., Yamashita, K., Ma, J.S., Lee, Y., Bando, H.,
945 Howard, J.C., Ebisu, S., Hayashi, M., *et al.* (2015). RabGDIalpha is a negative
946 regulator of interferon-gamma-inducible GTPase-dependent cell-autonomous
947 immunity to Toxoplasma gondii. *Proc Natl Acad Sci U S A* **112**(33), E4581-4590.
948 DOI: 10.1073/pnas.1510031112.
949 42. Okumi, H., and Koyama, A. (2014). Kampo medicine for palliative care in Japan.
950 *Biopsychosoc Med* **8**(1), 6. DOI: 10.1186/1751-0759-8-6.
951 43. Onishi, Y., Yamaura, T., Tauchi, K., Sakamoto, T., Tsukada, K., Nunome, S.,
952 Komatsu, Y., and Saiki, I. (1998). Expression of the anti-metastatic effect induced
953 by Juzen-taiho-to is based on the content of Shimotsu-to constituents. *Biol Pharm*
954 *Bull* **21**(7), 761-765. DOI: 10.1248/bpb.21.761.
955 44. Padgett, R.A., Grabowski, P.J., Konarska, M.M., Seiler, S., and Sharp, P.A. (1986).
956 Splicing of messenger RNA precursors. *Annu Rev Biochem* **55**, 1119-1150. DOI:
957 10.1146/annurev.bi.55.070186.005351.
958 45. Park, S.M., Kim, S.W., Jung, E.H., Ko, H.L., Im, C.K., Lee, J.R., Byun, S.H., Ku,
959 S.K., Kim, S.C., Park, C.A., *et al.* (2018). Sipjeondaebo-tang Alleviates Oxidative
960 Stress-Mediated Liver Injury through Activation of the CaMKK2-AMPK
961 Signaling Pathway. *Evid Based Complement Alternat Med* **2018**, 8609285. DOI:
962 10.1155/2018/8609285.
963 46. Patel, A.A., and Steitz, J.A. (2003). Splicing double: insights from the second
964 spliceosome. *Nat Rev Mol Cell Biol* **4**(12), 960-970. DOI: 10.1038/nrm1259.
965 47. Patwardhan, B., Warude, D., Pushpangadan, P., and Bhatt, N. (2005). Ayurveda
966 and traditional Chinese medicine: a comparative overview. *Evid Based*

967 *Complement Alternat Med* **2**(4), 465-473. DOI: 10.1093/ecam/neh140.
968 48. Pimentel, H., Parra, M., Gee, S.L., Mohandas, N., Pachter, L., and Conboy, J.G.
969 (2016). A dynamic intron retention program enriched in RNA processing genes
970 regulates gene expression during terminal erythropoiesis. *Nucleic Acids Res* **44**(2),
971 838-851. DOI: 10.1093/nar/gkv1168.
972 49. Razzaque, M.S. (2009). The FGF23-Klotho axis: endocrine regulation of
973 phosphate homeostasis. *Nat Rev Endocrinol* **5**(11), 611-619. DOI:
974 10.1038/nrendo.2009.196.
975 50. Robinson, J.T., Thorvaldsdottir, H., Winckler, W., Guttman, M., Lander, E.S., Getz,
976 G., and Mesirov, J.P. (2011). Integrative genomics viewer. *Nat Biotechnol* **29**(1),
977 24-26. DOI: 10.1038/nbt.1754.
978 51. Robinson, M.D., McCarthy, D.J., and Smyth, G.K. (2010). edgeR: a Bioconductor
979 package for differential expression analysis of digital gene expression data.
980 *Bioinformatics* **26**(1), 139-140. DOI: 10.1093/bioinformatics/btp616.
981 52. Rui, L. (2014). Energy metabolism in the liver. *Compr Physiol* **4**(1), 177-197. DOI:
982 10.1002/cphy.c130024.
983 53. Saiki, I. (2000). A Kampo medicine "Juzen-taiho-to"--prevention of malignant
984 progression and metastasis of tumor cells and the mechanism of action. *Biol*
985 *Pharm Bull* **23**(6), 677-688. DOI: 10.1248/bpb.23.677.
986 54. Saiki, I., Koizumi, K., Goto, H., Inujima, A., Namiki, T., Raimura, M., Kogure, T.,
987 Tatsumi, T., Inoue, H., Sakai, S., *et al.* (2013). The long-term effects of a kampo
988 medicine, juzentaihoto, on maintenance of antibody titer in elderly people after
989 influenza vaccination. *Evid Based Complement Alternat Med* **2013**, 568074. DOI:
990 10.1155/2013/568074.
991 55. Shalgi, R., Hurt, J.A., Lindquist, S., and Burge, C.B. (2014). Widespread inhibition
992 of posttranscriptional splicing shapes the cellular transcriptome following heat
993 shock. *Cell Rep* **7**(5), 1362-1370. DOI: 10.1016/j.celrep.2014.04.044.
994 56. Shen, S., Park, J.W., Lu, Z.X., Lin, L., Henry, M.D., Wu, Y.N., Zhou, Q., and Xing,
995 Y. (2014). rMATS: robust and flexible detection of differential alternative splicing
996 from replicate RNA-Seq data. *Proc Natl Acad Sci U S A* **111**(51), E5593-5601.
997 DOI: 10.1073/pnas.1419161111.
998 57. Shoemaker, J.E., Lopes, T.J.S., Ghosh, S., Matsuoka, Y., Kawaoka, Y., and Kitano,
999 H. (2012). CTen: a web-based platform for identifying enriched cell types from
1000 heterogeneous microarray data. *BMC Genomics* **13**(1), 460. DOI: 10.1186/1471-
1001 2164-13-460.
1002 58. Solana, R., Pawelec, G., and Tarazona, R. (2006). Aging and innate immunity.

1003 *Immunity* **24**(5), 491-494. DOI: 10.1016/j.immuni.2006.05.003.
1004 59. Stegeman, R., and Weake, V.M. (2017). Transcriptional Signatures of Aging. *J Mol*
1005 *Biol* **429**(16), 2427-2437. DOI: 10.1016/j.jmb.2017.06.019.
1006 60. Takeno, N., Inujima, A., Shinohara, K., Yamada, M., Shibahara, N., Sakurai, H.,
1007 Saiki, I., and Koizumi, K. (2015). Immune adjuvant effect of Juzentaihoto, a
1008 Japanese traditional herbal medicine, on tumor vaccine therapy in a mouse model.
1009 *Int J Oncol* **47**(6), 2115-2122. DOI: 10.3892/ijo.2015.3208.
1010 61. Trapnell, C., Pachter, L., and Salzberg, S.L. (2009). TopHat: discovering splice
1011 junctions with RNA-Seq. *Bioinformatics* **25**(9), 1105-1111. DOI:
1012 10.1093/bioinformatics/btp120.
1013 62. Ullrich, S., and Guigo, R. (2019). Dynamic changes in intron retention are tightly
1014 associated with regulation of splicing factors and proliferative activity during B-
1015 cell development. *Nucleic Acids Res*. DOI: 10.1093/nar/gkz1180.
1016 63. UNESCO (2011). Huang Di Nei Jing (Yellow Emperor's Inner Canon) (Beijing:
1017 National Library of China ).
1018 64. Vu, T.-D., Iwasaki, Y., Shigenobu, S., Maruko, A., Oshima, K., Iioka, E., Huang,
1019 C-L. Abe, T., Tamaki, S., Lin, Y-W., Chen, C-K., Lu, M-Y., Hojo, M., Wang, H-
1020 V., Tzeng, S-F., Huang, H-J., Kanai, A,, Gojobori, T., Chiang, T-Y., Sun, H.S., Li,
1021 W-H., Okada, N. (2019). Behavioral and neurotranscriptomic synchronization
1022 between the two opponents of a fighting pair of the fish Betta splendens. *PLOS*
1023 *Biology.* submitted.
1024 65. Wang, Z., Qi, F., Cui, Y., Zhao, L., Sun, X., Tang, W., and Cai, P. (2018). An update
1025 on Chinese herbal medicines as adjuvant treatment of anticancer therapeutics.
1026 *Biosci Trends* **12**(3), 220-239. DOI: 10.5582/bst.2018.01144.
1027 66. Weischenfeldt, J., Lykke-Andersen, J., and Porse, B. (2005). Messenger RNA
1028 surveillance: neutralizing natural nonsense. *Curr Biol* **15**(14), R559-562. DOI:
1029 10.1016/j.cub.2005.07.002.
1030 67. Wong, J.J., Ritchie, W., Ebner, O.A., Selbach, M., Wong, J.W., Huang, Y., Gao, D.,
1031 Pinello, N., Gonzalez, M., Baidya, K.*, et al.* (2013). Orchestrated intron retention
1032 regulates normal granulocyte differentiation. *Cell* **154**(3), 583-595. DOI:
1033 10.1016/j.cell.2013.06.052.
1034 68. Xu, W., Wei, Z., Dong, J., Duan, F., Chen, K., Chen, C., Liu, J., Yang, X., Chen,
1035 L., Xiao, H.*, et al.* (2017). Global Metabolomics Reveals the Metabolic
1036 Dysfunction in Ox-LDL Induced Macrophage-Derived Foam Cells. *Front*
1037 *Pharmacol* **8**, 586. DOI: 10.3389/fphar.2017.00586.
1038 69. Yeo, G., and Burge, C.B. (2004). Maximum entropy modeling of short sequence

1039 motifs with applications to RNA splicing signals. *J Comput Biol* **11**(2-3), 377-394.
1040 DOI: 10.1089/1066527041410418.
1041 70. Yoshioka, H., Fukaya, S., Miura, N., Nagatsu, A., and Nonogaki, T. (2016).
1042 Hepatoprotective effect of kampo formula "Juzen-taiho-to" on bromobenzene-
1043 induced toxicity in mice. *Fundamental Toxicological Sciences* **3**(5), 233-236.
1044 DOI: 10.2131/fts.3.233.
1045 71. Yoshioka, H., Fukaya, S., Tominaga, S., Nagatsu, A., Miura, N., and Maeda, T.
1046 (2019). Protective effect of the Kampo formula "Juzen-taiho-to" on isoniazid- and
1047 rifampicin-induced hepatotoxicity in mice. *Fundamental Toxicological Sciences*
1048 **6**(1), 25-29. DOI: 10.2131/fts.6.25.
1049 72. Zane, L., Sharma, V., and Misteli, T. (2014). Common features of chromatin in
1050 aging and cancer: cause or coincidence? *Trends Cell Biol* **24**(11), 686-694. DOI:
1051 10.1016/j.tcb.2014.07.001.
1052 73. Zelcer, N., and Tontonoz, P. (2006). Liver X receptors as integrators of metabolic
1053 and inflammatory signaling. *J Clin Invest* **116**(3), 607-614. DOI:
1054 10.1172/JCI27883.
1055 74. Zhang, J., and Manley, J.L. (2013). Misregulation of pre-mRNA alternative
1056 splicing in cancer. *Cancer Discov* **3**(11), 1228-1237. DOI: 10.1158/2159-
1057 8290.CD-13-0253.
1058 75. Zheng, H.C., Noguchi, A., Kikuchi, K., Ando, T., Nakamura, T., and Takano, Y.
1059 (2014). Gene expression profiling of lens tumors, liver and spleen in alpha-
1060 crystallin/SV40 T antigen transgenic mice treated with Juzen-taiho-to. *Mol Med*
1061 *Rep* **9**(2), 547-552. DOI: 10.3892/mmr.2013.1854.
1062 76. Zhou, X., Seto, S.W., Chang, D., Kiat, H., Razmovski-Naumovski, V., Chan, K.,
1063 and Bensoussan, A. (2016). Synergistic Effects of Chinese Herbal Medicine: A
1064 Comprehensive Review of Methodology and Current Research. *Front Pharmacol*
1065 **7**, 201. DOI: 10.3389/fphar.2016.00201.
1066
1067

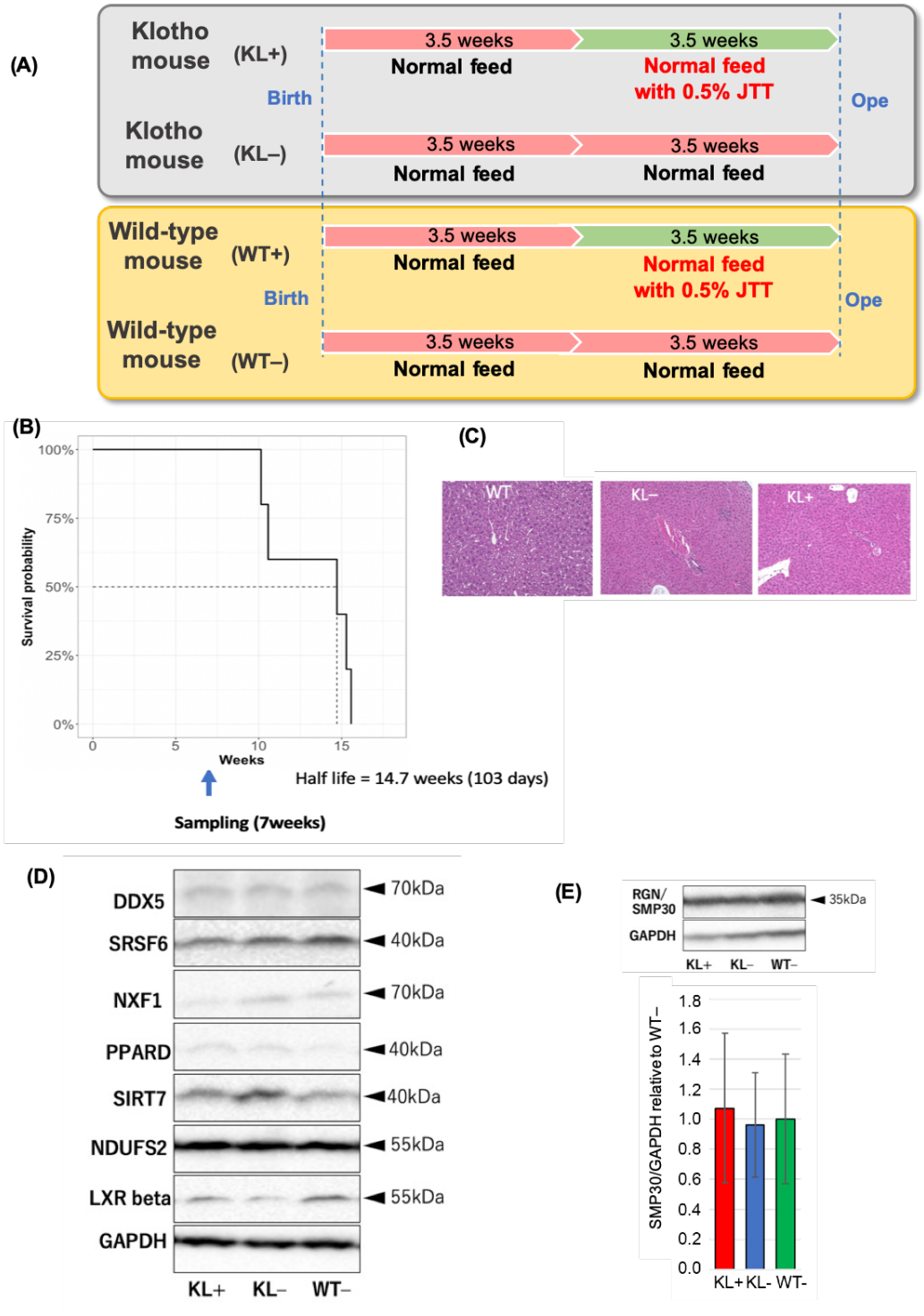


**Figure 1. Klotho mice at 7 weeks of age represent the pre-disease state**

(A) Schematic illustration of animal experiments. Three-week-old male α-klotho knockout (*Kl*$^{-/-}$/Jcl) mice (klotho mice) (n = 8) and WT (C57BL/6JJcl) mice (n = 8) were purchased from CLEA Japan, Tokyo, Japan. The mice were acclimated for 0.5 weeks in a vinyl isolator, during which they were given radiation-sterilized water and

1074 CE-2 diet (CLEA Japan) ad libitum. Thereafter, the klotho mice and WT mice were
1075 each divided into two groups, with four animals in each. In each case, one group of
1076 mice was fed CE-2 containing 0.5% (w/w) JTT, whereas the other group was fed CE-2
1077 only from 3.5 weeks of age until the mice were 7 weeks old. Ope stands for operation.
1078 (B) Estimation of the half-life of klotho mice. N = 5. (C) Histological observations of
1079 liver tissues from KL+ and KL− showed that they did not exhibit any signs of aging
1080 relative to WT mice. (D) The expression of seven proteins, each of which showed IR,
1081 was examined by western blotting. Expression levels did not change in KL+, KL−, and
1082 WT− at 7 weeks of age. (E) Representative western blotting data (upper) of a
1083 senescence marker protein, RGN/SMP30, together with its quantified expression
1084 (lower) show that KL− are not senescent. Statistical significance was estimated by one-
1085 way ANOVA. Error bars indicate mean ±standard deviations of triplicate
1086 measurements.
1087
1088

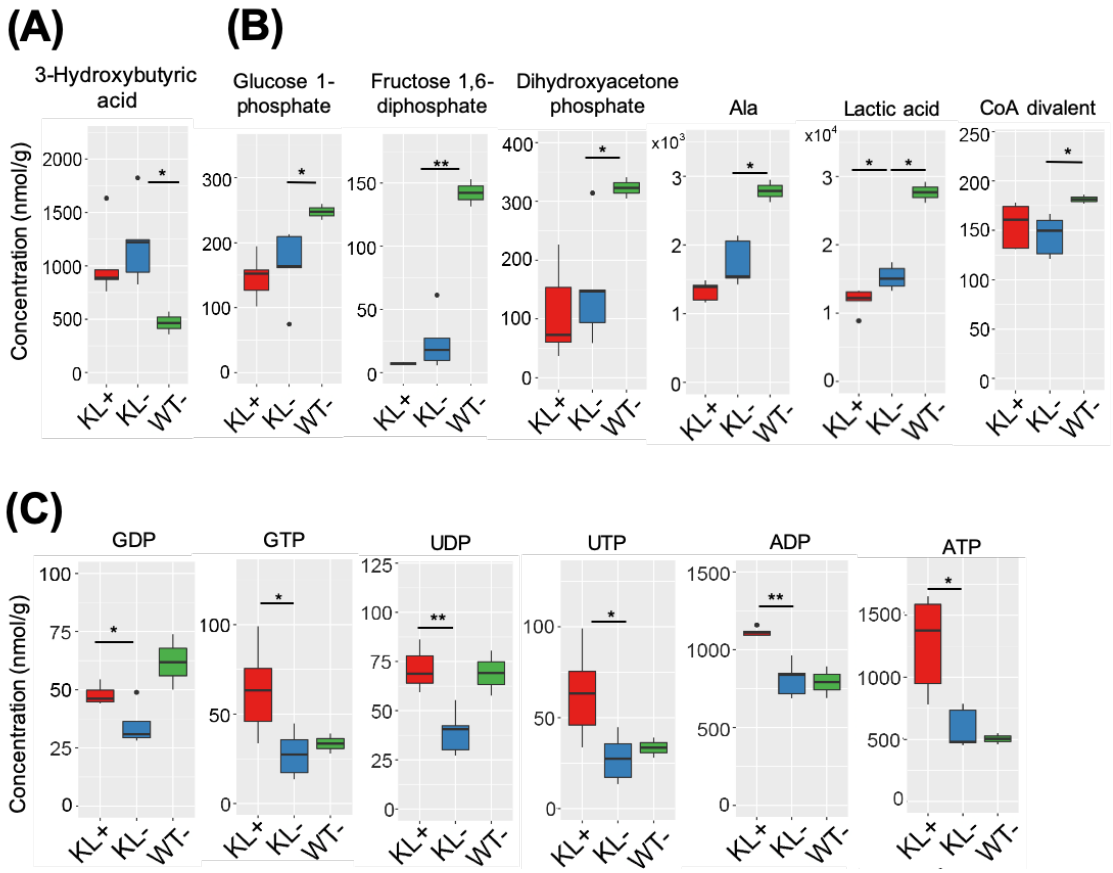


**Figure 2. A metabolome analysis showed that the klotho mice are undergoing a starvation-like condition at 7 weeks of age**

Based on a metabolome analysis of (A) 3-HBA and (B) other glycolysis-related metabolites, KL– data indicate that these mice are undergoing a starvation-like condition. *P ≤ 0.05, **P ≤ 0.001, unpaired Student's t-test. Based on the metabolome analysis about metabolites related to RNA precursors, the concentrations of some nucleotides were recovered in KL+ in comparison with KL– and WT–. *P ≤ 0.05, **P ≤ 0.001, unpaired Student's t-test.

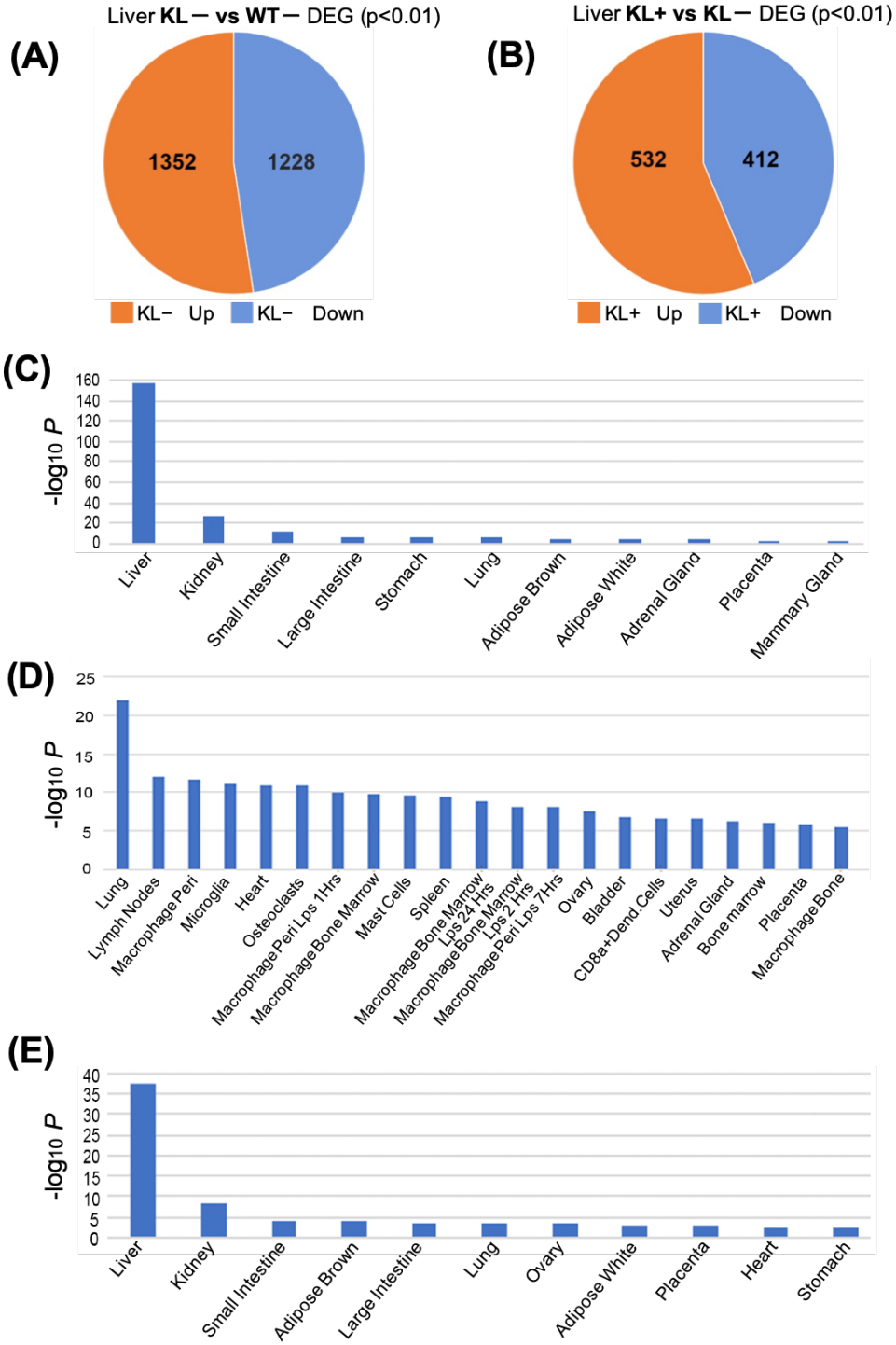
(A)
Liver KL− vs WT− DEG (p<0.01)
1352
1228
KL− Up
KL− Down
(B)
Liver KL+ vs KL− DEG (p<0.01)
532
412
KL+ Up
KL+ Down
(C)
-log10 P
160
140
120
100
80
60
40
20
0
Liver
Kidney
Small Intestine
Large Intestine
Stomach
Lung
Adipose Brown
Adipose White
Adrenal Gland
Placenta
Mammary Gland
(D)
-log10 P
25
20
15
10
5
0
Lung
Lymph Nodes
Macrophage Peri
Microglia
Heart
Osteoclasts
Macrophage Peri Lps 1Hrs
Macrophage Bone Marrow
Mast Cells
Spleen
Macrophage Bone Marrow Lps 24 Hrs
Macrophage Bone Marrow Lps 2 Hrs
Macrophage Peri Lps 7Hrs
Ovary
Bladder
CD8a+Dend Cells
Uterus
Adrenal Gland
Bone marrow
Placenta
Macrophage Bone
(E)
-log10 P
40
35
30
25
20
15
10
5
0
Liver
Kidney
Small Intestine
Adipose Brown
Large Intestine
Lung
Ovary
Adipose White
Placenta
Heart
Stomach

1101
1102

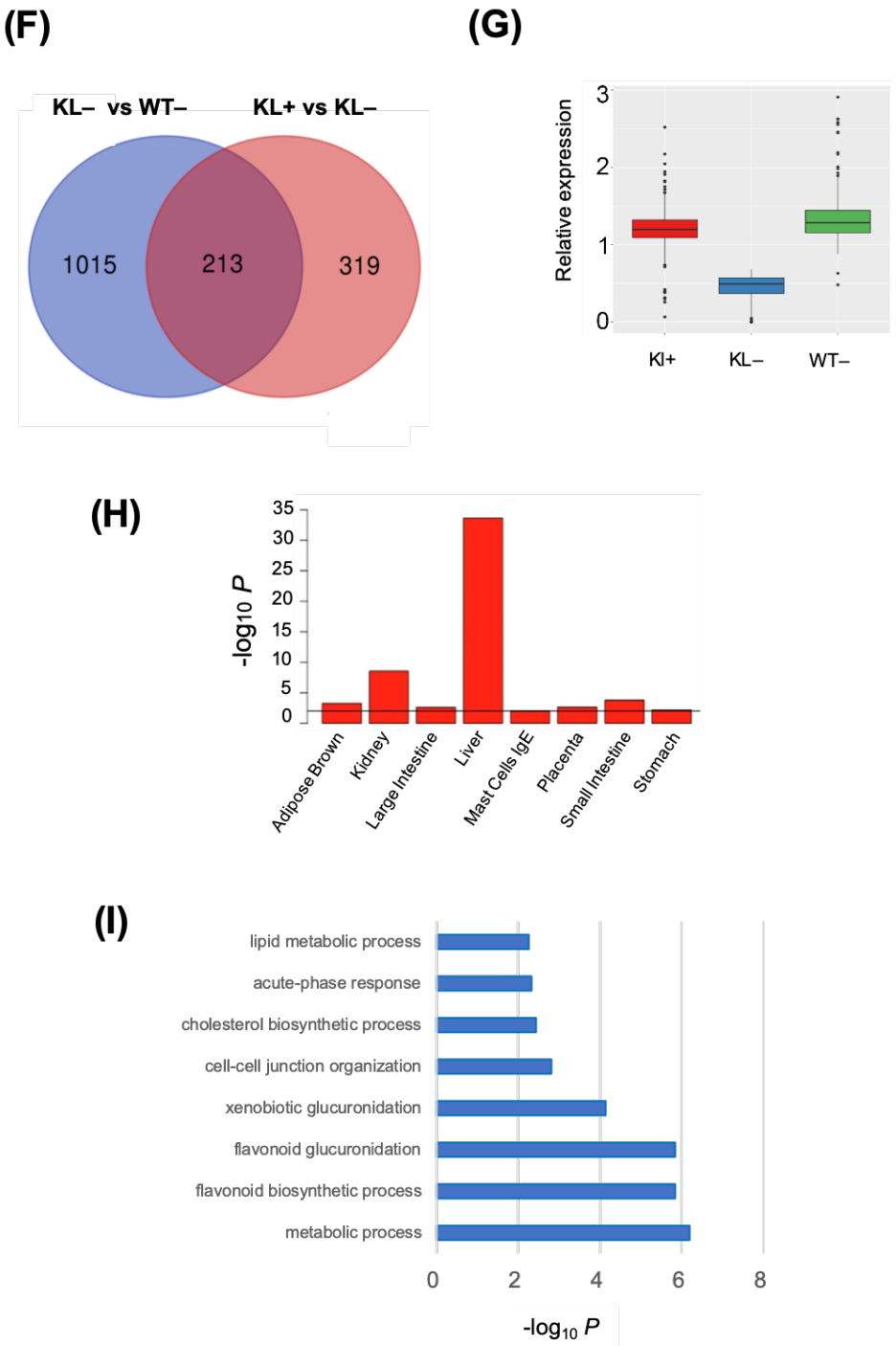


**Figure 3. DEG analysis showed that liver function in klotho mice improved after administration of JTT**

Number of up-regulated genes and down-regulated genes from the DEG data for the comparison (A) of KL– vs WT– and (B) of KL+ vs KL–. Cten analysis of (C) 1228 down-regulated genes in KL– in the comparison of KL– vs WT–, (D) 1352 up-regulated

genes in KL–in the comparison of KL– vs WT–, and (E) 532 up-regulated genes in KL+ in the comparison of KL+ vs KL–. (F) A Venn diagram of transcriptome comparisons from KL+ vs KL– and KL– vs WT–. Two hundred thirteen genes were shared between the comparisons. (G) Box plots of 213 gene expression data show a significant decrease in KL– in comparison with that in WT– and a significant increase in KL+ in comparison with KL–. Values along the vertical axis are normalized based on the overall average. (H) Cten analysis (http://www.influenza-x.org/~jshoemaker/cten/) for 213 genes that were differentially expressed in the comparison between KL+ vs KL– and between KL– vs WT–. The horizontal line indicates $P = 0.01$. (I) Bar graphs showing $-\log_{10} P$ of GO terms enriched for the 213 genes shown in (F). Only those terms with $P < 0.01$ are shown.

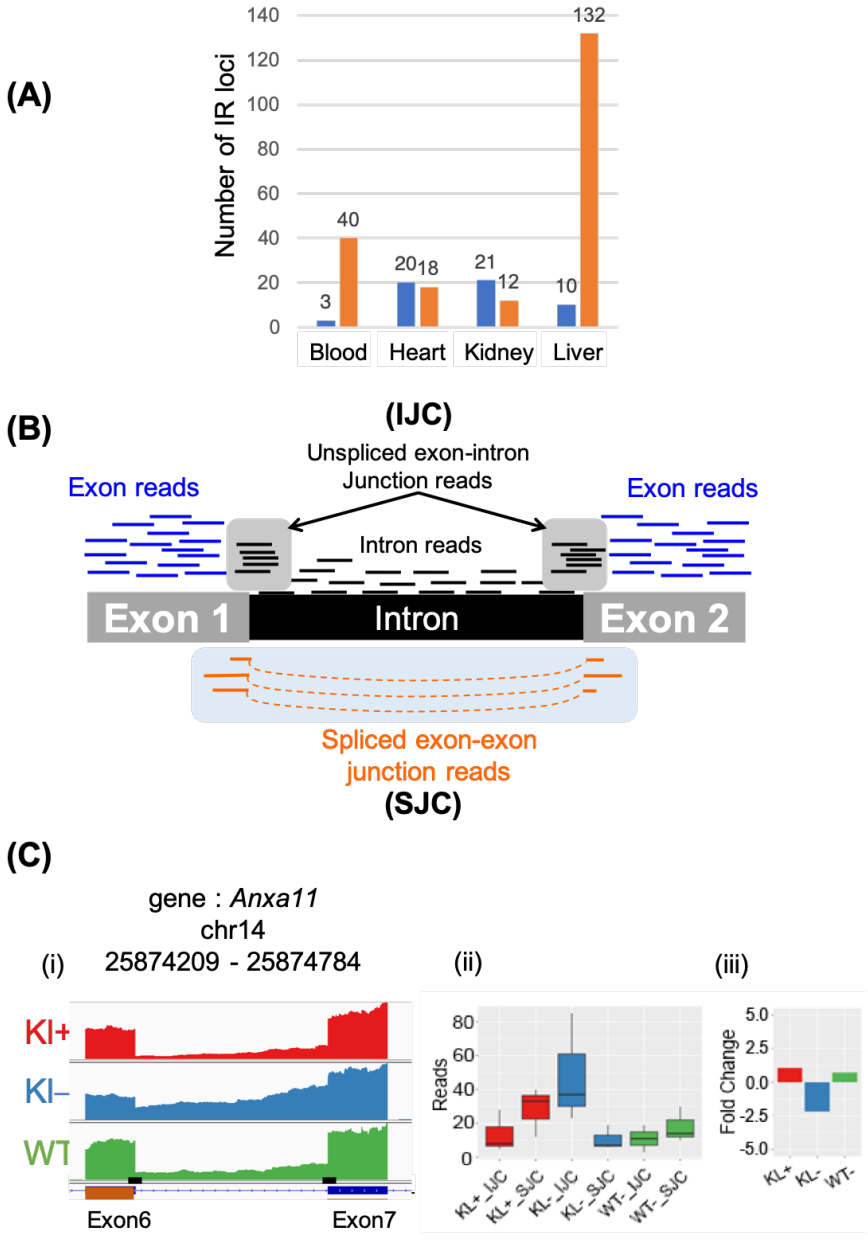


**Figure 4. Quantification of IR events**

(A) Among the four organs examined, liver had the most notable recovery of retained introns after administration of JTT. Bar graphs show the number of retained introns that decreased (in orange) or increased (in blue) in the four organs as a result of administration of JTT. Based on the rMATS analysis, genes with a significant change in IR in the comparison of KL+ vs KL– were divided into two groups. In the liver, the first group includes genes that showed a decrease in IR in KL+ (132 loci; DecIR type, implying that the fold change of KL+ was larger than that of KL–), and the second

includes genes with an increase in IR in KL+ (10 loci; IncIR type, implying that the fold change of KL+ was smaller than that of KL–). (B) The quantification of IR events from mRNA-seq data using rMATS. The IJCs represent the reads containing the intron sequence at the junction. The SJCs represent the reads without intron sequences at the junction. (C) (i) The mapping results from KL+, KL–, and WT– are shown for a single gene, *Anxa11*, using Integrative Genomics Viewer (IGV). Thick black bars indicate the sites of junctions in the reads where SJCs and IJCs were analyzed. (ii) Read counts from KL+, KL–, and WT– for IJCs and SJCs. (iii) FC in the number of SJCs relative to IJCs for KL+, KL–, and WT–.

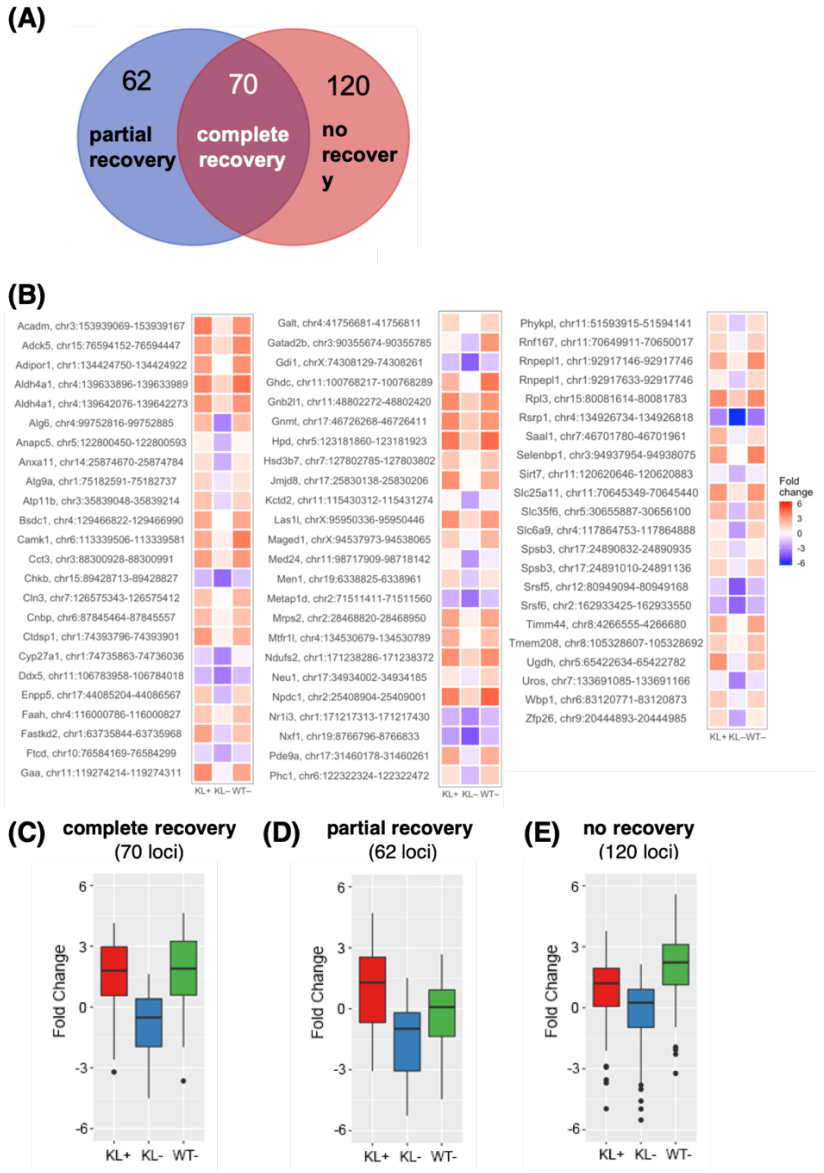


**Figure 5. Seventy loci of complete recovery show a typical V-shaped pattern of recovery**

(A) A Venn diagram of two types of loci, the DecIR type (blue circle) in the comparison of KL+ and KL– and the IncIR type (red circle) in the comparison of KL– and WT–. Three categories, namely "partial recovery", "complete recovery", and "no recovery" loci, are distinguishable. (B) Heat map illustration of FC values of loci in KL+, KL–, and WT– for the 70 "complete recovery" loci. (C–E) Boxplots of the FC values of (C) the 70 "complete recovery" loci, (D) the 62 "partial recovery" loci, and (E) the 120 "no-recovery" loci in KL+, KL–, and WT–.

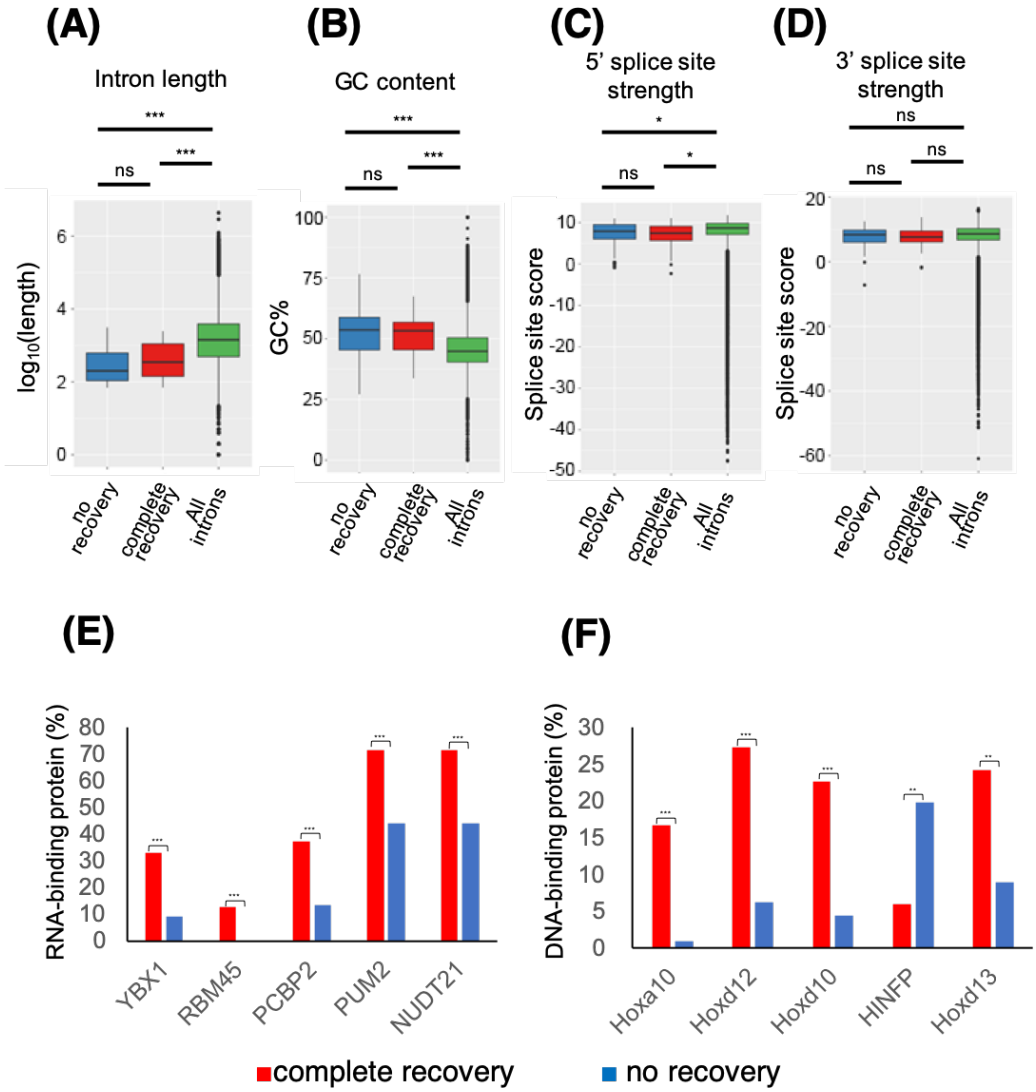


**Figure 6. Retained intron loci have distinguishing characteristics**

(A–D) Boxplots showing (A) intron lengths, (B) the GC percentage in intron sequences, and the strength score of the (C) 5' and (D) 3' splice sites compared among three groups of introns, namely "no recovery", "complete recovery", and all introns from liver-expressed genes (254,005 loci). *$P \leq 0.05$, ***$P \leq 0.001$, unpaired Student's *t*-test; ns, not significant. (E, F) Bar graphs showing percentage of loci in the "complete recovery" and "no recovery" groups that have (E) motifs for RNA-binding proteins within the intron or (F) motifs for DNA-binding proteins in the promoter region. **$P \leq 0.01$, ***$P \leq 0.001$, Fisher's test.

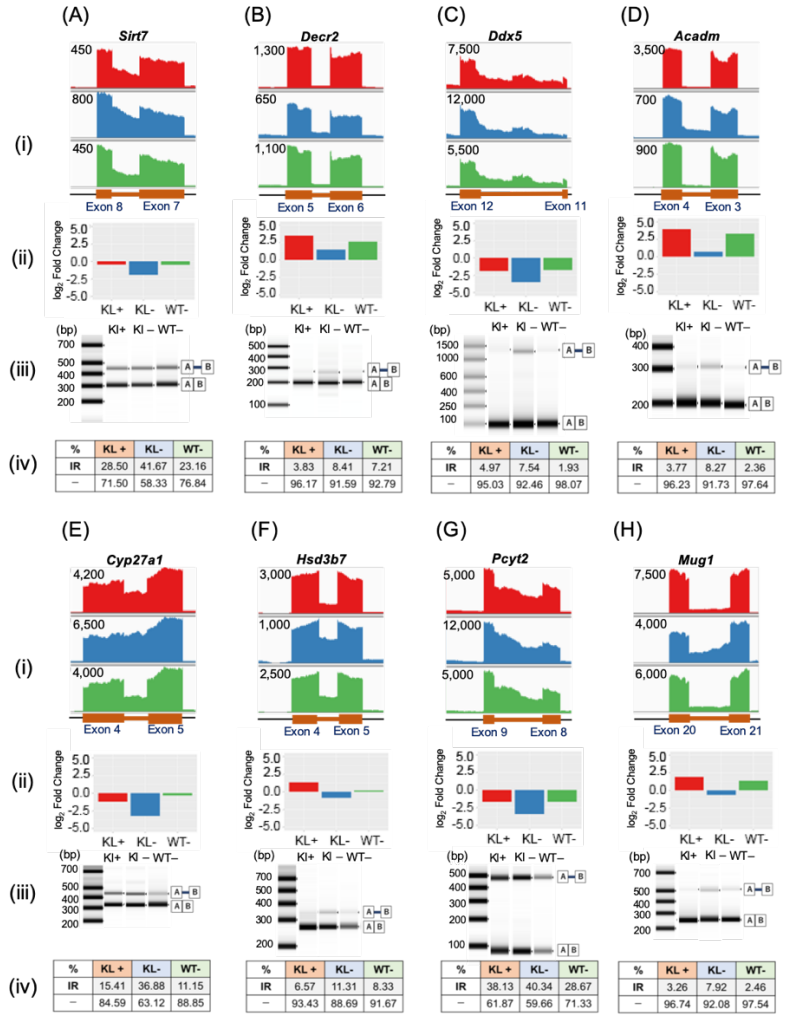


**Figure 7. RT-PCR validation of retained introns and their recovery after administration of JTT**

(A–H) Eight genes, (A) *Sirt7*, (B) *Decr2*, (C) *Ddx5*, (D) *Acadm*, (E) *Cyp27a1*, (F) *Hsd3b7*, (G) *Pcyt2*, and (H) *Mug1*, were subjected to the following analyses. (i) IGV mapping of reads from KL+, KL–, and WT–. The numbers shown to the left of each map represent read counts. (ii) Bar graphs showing fold changes in SJCs relative to IJCs for KL+, KL–, and WT–. (iii) RT-PCR validation of RNA expression from KL+, KL–, and WT–. A and B indicate exons, with the intervening intron indicated for the higher-molecular-weight product. (iv) The ratio of each transcript as determined using TapeStation. Data from KL+, KL–, and WT– are shown in red, blue, and green, respectively.

1187

**(A)**

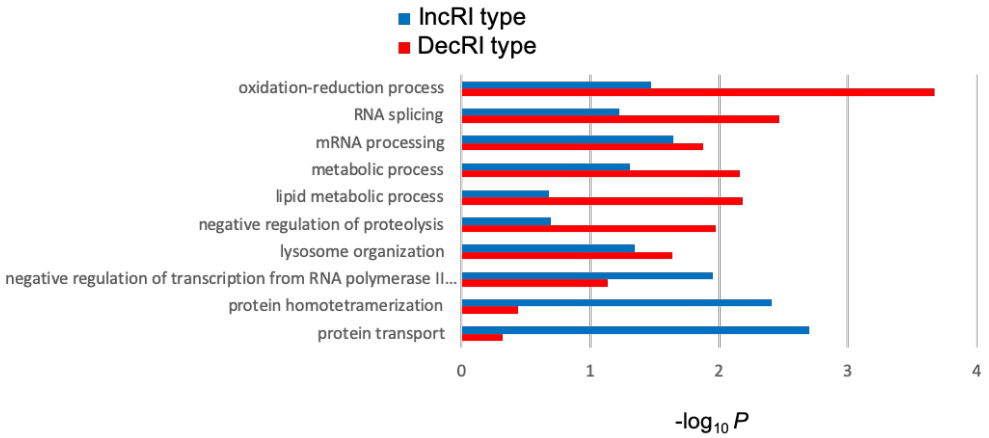


**(B)**

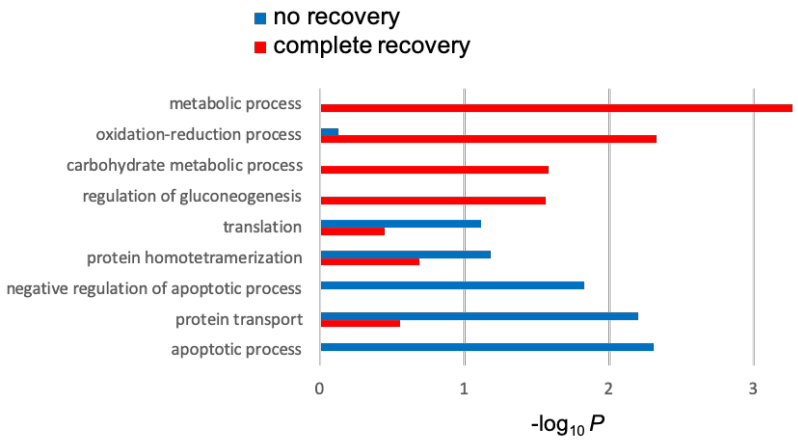


**(C)**

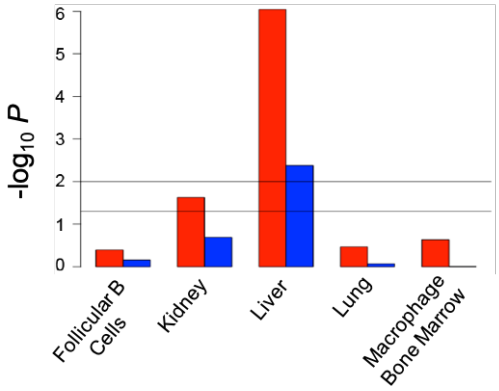


1188

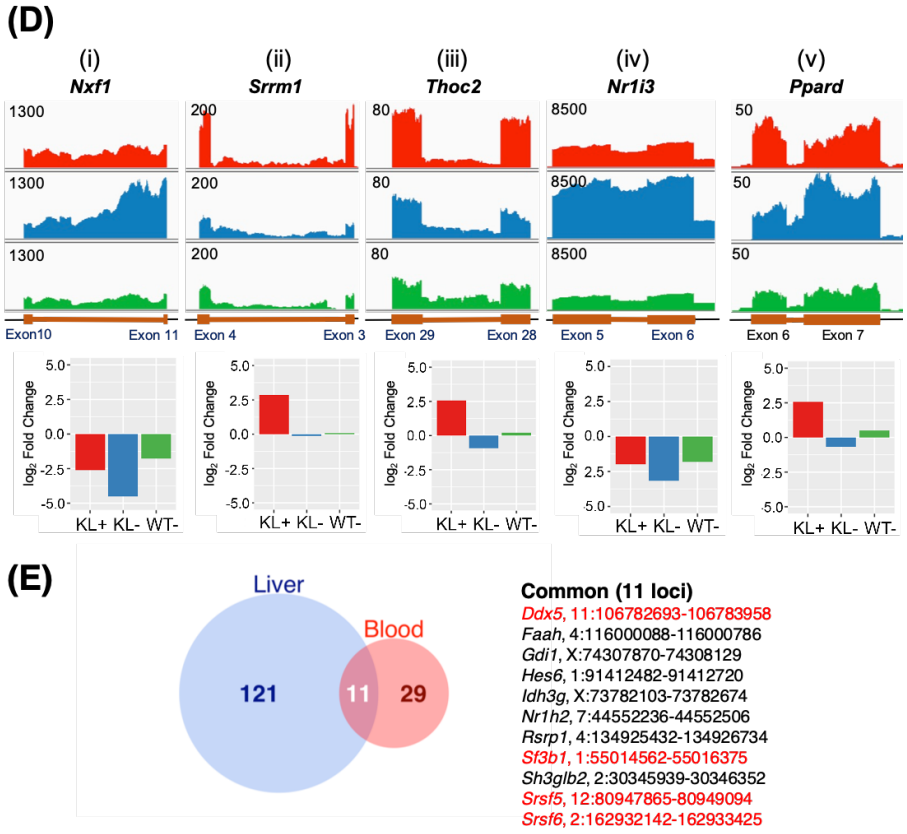


**Figure 8. Genes with recovered retained introns in liver have the characteristics of liver-specific genes.**

(A) Bar graphs showing $-\log_{10} P$ of GO terms enriched for genes whose IR events were significantly changed in the liver. Red bars show enrichment of GO terms in genes with the DecIR type in KL+ in the KL+ and KL– comparison, and blue bars show enrichment of GO terms in genes with the IncIR type in KL– in the KL– and WT– comparison. (B) Bar graphs showing $-\log_{10} P$ of GO terms enriched for genes defined as "complete recovery" (red bars) and "no recovery" (blue bars) loci. (C) Cten analysis for genes expressed in the liver with the DecIR type in red and those with the IncIR type in blue as shown in Fig. 5A. Horizontal lines indicate $P = 0.05$ (lower line) and 0.01 (upper line). (D) The mapping results from IGV for five gene loci, (i) *Nxf1*, (ii) *Srrm1*, (iii) *Thoc2*, (iv) *Nr1i3*, and (v) *Ppard*, are shown (upper). Bar graphs (lower) show the FC using the IJC and SJC values for KL+, KL–, and WT–. (E) Eleven genes were shared in common between the liver and blood in the recovery process of IR after administration of JTT. The Venn diagram (left) of the DecIR genes that were shared in the liver and the blood. The overlapping genes between blood and liver are listed (right), among which splicing-related genes are shown in red.

1208

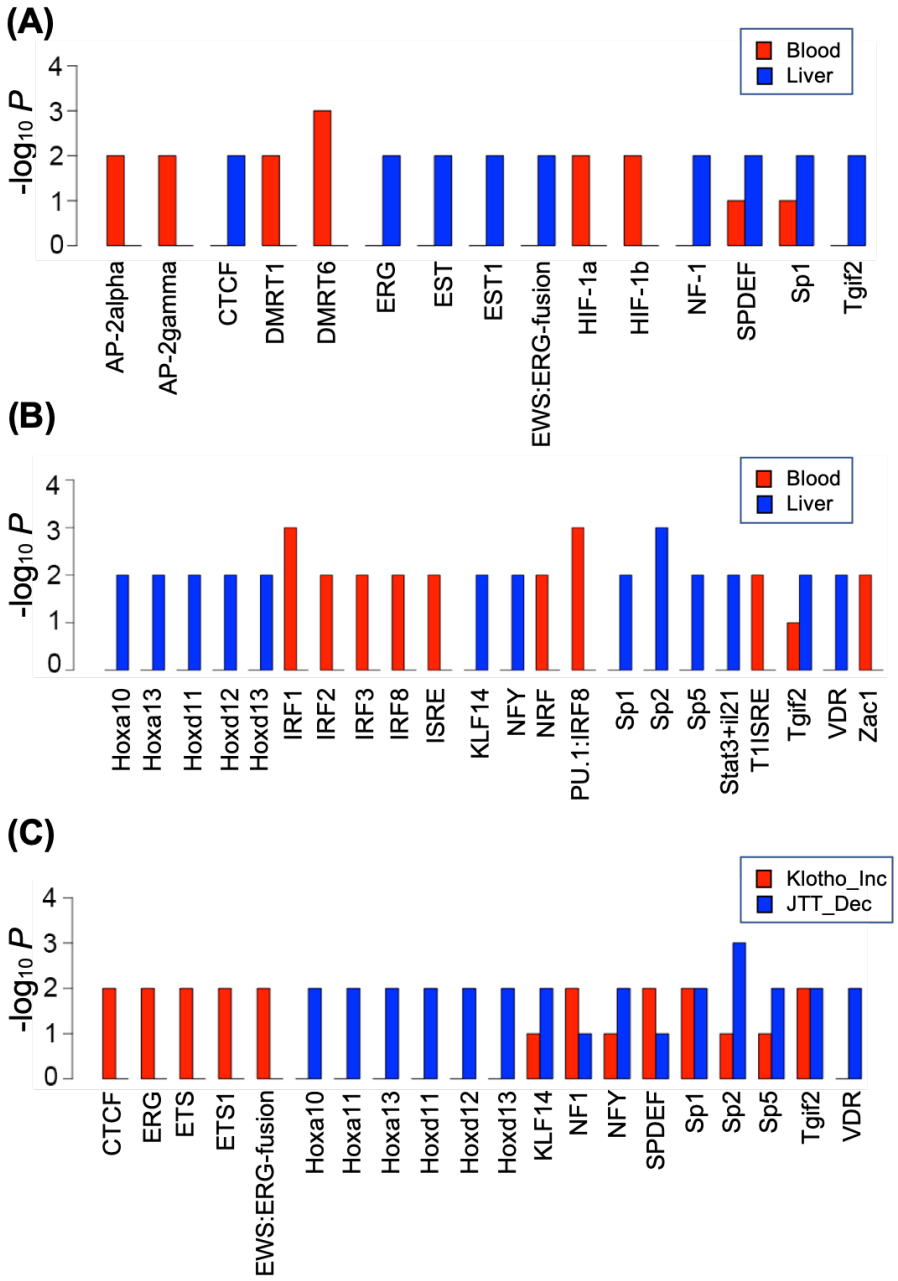


1209
1210
1211

**(D)**

(i)

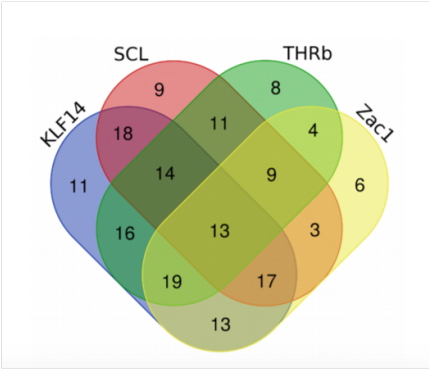


(ii)

| TF | num of genes |
|---|---|
| KLF14(Zf) | 121 |
| Sp2(Zf) | 120 |
| Sp5(Zf) | 104 |
| KLF5(Zf) | 102 |
| SCL(bHLH) | 94 |
| THRb(NR) | 92 |
| Zac1(Zf) | 84 |
| KLF6(Zf) | 83 |
| ETV1(ETS) | 82 |
| AR-halfsite(NR) | 81 |

**(E)**

(i)

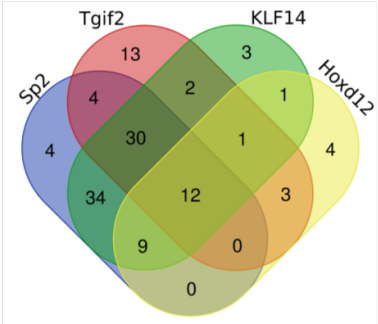


(ii)

| TF | num of genes |
|---|---|
| Sp2(Zf) | 93 |
| KLF14(Zf) | 92 |
| Sp5(Zf) | 79 |
| Tgif2(Homeobox) | 65 |
| Sp1(Zf) | 52 |
| NFY(CCAAT) | 45 |
| Hoxd11(Homeobox) | 43 |
| Hoxa13(Homeobox) | 42 |
| Hoxa11(Homeobox) | 40 |
| Hoxd13(Homeobox) | 31 |

**Figure 9. A very few TFs may control genes with DecIR as well as those with IncIR** (A) Bar graphs showing $-\log_{10}P$ of enrichment of the TF-binding motif in genes with IncIR from blood and liver. (B) Bar graphs showing $-\log_{10}P$ of enrichment of the TF-binding motif in genes with DecIR from blood and liver. (C) Bar graphs showing $-\log_{10}P$ of enrichment of the TF-binding motif in genes with IncIR and DecIR from liver. (D) Genes with IncIR may be controlled by a very few TFs. (i) Venn diagrams of the IncIR genes that have TF-binding motifs in the liver and (ii) the top 10 motifs represented in these genes. (E) Genes with DecIR may be controlled by a very few TFs. (i) Venn diagrams of the DecIR genes that have TF-binding motifs in the liver and (ii) the top 10 motifs represented in these genes.

1226

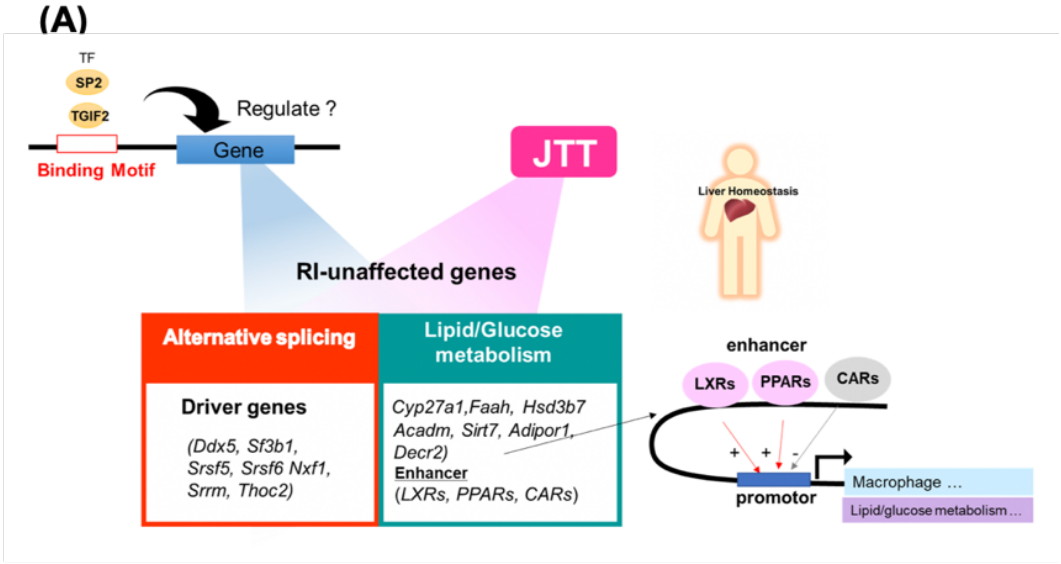


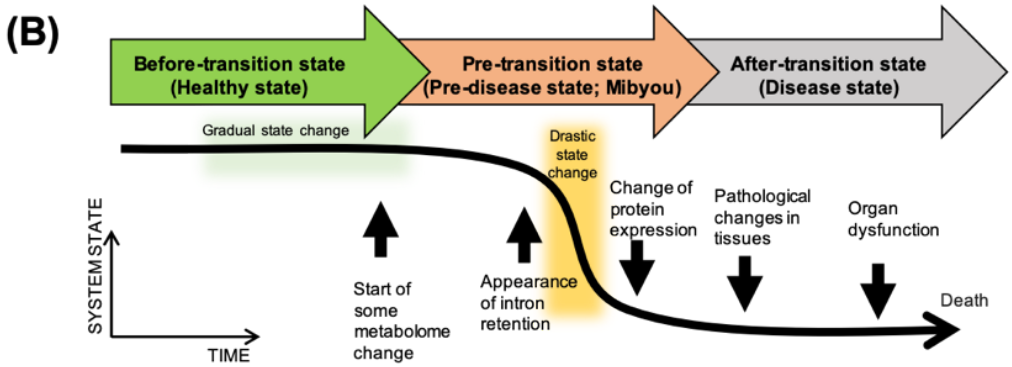


1227

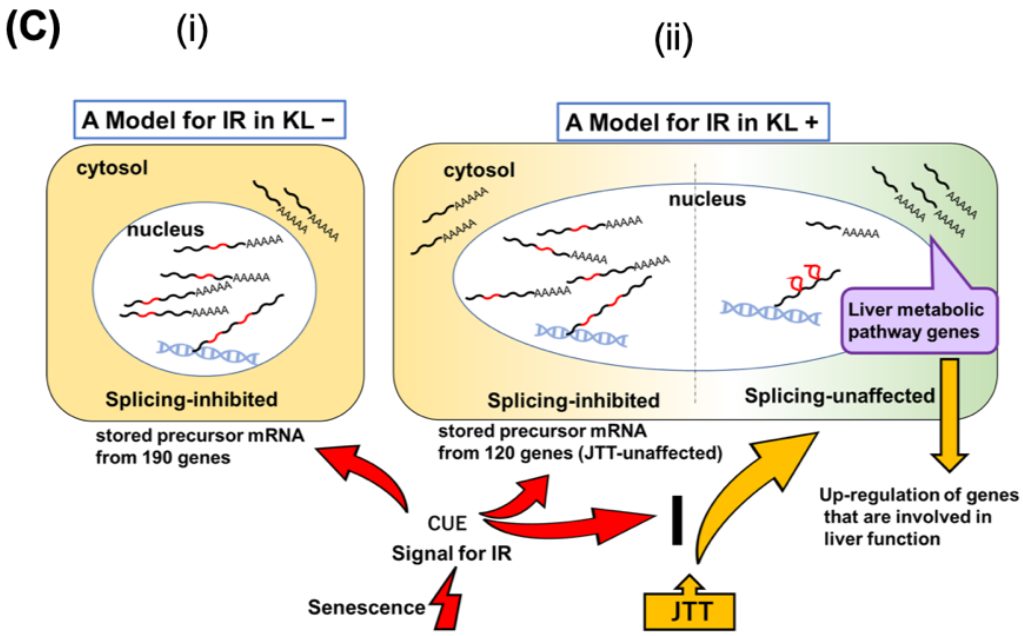


1228

1229 **Figure 10. IR is a marker of the pre-disease state and the recovery of retained**
1230 **introns suggests the recovery to the normal state.**
1231 (A) Illustration of the functional orchestration of IR-recovered genes under surveillance
1232 of homeostasis within the host. Two categories of genes that are involved are shown:
1233 alternative splicing and the biological function lipid/glucose metabolism. We
1234 hypothesize that the surveillance of homeostasis affects which genes undergo IR
1235 recovery after JTT administration during the earlier stage of aging (7 weeks of age)
1236 from the pre-disease state to the normal state (see the Discussion). Except for genes for
1237 alternative splicing and lipid/glucose metabolism, several genes involved in
1238 mitochondria function and the immune system including macrophage function were
1239 included among 124 IR-recovered genes (Fig. 5A; 132 loci). *Polrmt*, *Uros*, *Sh3glb2*,
1240 *Idh3*, *Cyp27a1*, and *Hsd3b7* are involved in mitochondrial function. JTT protects
1241 mitochondrial function (Park et al., 2018), and a JTT-related multi-herbal medicine
1242 prevents mitochondrial dysfunction, providing a possible treatment for the prevention of
1243 Parkinson disease (Ko et al., 2018). In addition, the anti-tumor effect of JTT may rely
1244 partly on activation of mitochondria (Zheng et al., 2014). *Gdi1*, *Sh3glb2*, *Faah*, and
1245 LXRβ are involved in the immune system including macrophage function and interferon
1246 activity. JTT has been widely used as a palliative to treat cancer patients (Okumi and
1247 Koyama, 2014) and also to treat patients with bacterial infections such as acute otitis
1248 media (Kitamura et al., 2015). JTT also contributes to the maintenance of antibody titer
1249 in elderly people after influenza vaccination (Saiki et al., 2013). A number of animal
1250 studies have demonstrated an adjuvant effect of JTT, especially with respect to
1251 activation of innate immune cells such as macrophages, dendritic cells, natural killer
1252 cells, and natural killer T cells (Ishikawa et al., 2017). Microarray analysis indicates that
1253 the target of JTT might be the transcription machinery regulating the steady-state level
1254 of the type 1 interferon-related genes (Munakata et al., 2012). Oral administration of
1255 JTT can elevate the phagocytic activity of macrophage-like cells in the various tissues
1256 (Saiki, 2000, Takeno et al., 2015). Similarly, the phytoestrogen flavonoids found in
1257 Glycyrrhizae radix, one of the components of JTT, can enhance phagocytosis in a
1258 murine macrophage cell line, as we described previously (Kaneko et al., 2017). JTT
1259 contains various types of flavonoids, some of which have been identified as selective
1260 agonists of LXR, according to molecular-docking analysis *in silico* (Fouache et al.,
1261 2019). LXRs, PPARs, and CARs are nuclear receptors and regulate genes related to
1262 lipid/glucose metabolism and macrophage function. (B) Schematic representation of the
1263 disease process from the healthy state through the pre-disease state. Possible changes
1264 that occur in the body are shown with arrows. (C) A model to explain why a specific

1265 subset of genes with IR was recovered in KL+ by administration of JTT. (i) In the case
1266 of KL−, it is presumed that ~200 pre-mRNAs containing retained introns were stored in
1267 the nucleus because of the stress signal induced by aging so that the cells can save
1268 energy. (ii) In the case of KL+, as liver metabolic stress was recovered after JTT
1269 administration, the improved condition of the liver cells led to enhanced post-
1270 transcriptional splicing among pre-mRNAs with retained introns involved in
1271 metabolism.
1272

1273

1274 **Table 1-1.** Number of alternative splicing loci between KL+ and KL−

| | A3SS | | A5SS | | SE | | IR | | MXE | | Total | |
|---|---|---|---|---|---|---|---|---|---|---|---|---|
| | $P < 0.01$ | FDR <0.05 | $P < 0.01$ | FDR < 0.05 | $P < 0.01$ | FDR <0.05 | $P < 0.01$ | FDR <0.05 | $P < 0.01$ | FDR <0.05 | $P < 0.01$ | FDR <0.05 |
| **Blood** | 16 | 1 | 13 | 4 | 58 | 6 | 69 | 10 | 4 | 0 | 160 | 21 |
| **Kidney** | 17 | 2 | 13 | 5 | 96 | 18 | 33 | 9 | 3 | 1 | 162 | 35 |
| **Heart** | 16 | 0 | 3 | 3 | 90 | 2 | 38 | 5 | 7 | 1 | 154 | 11 |
| **Liver** | 63 | 16 | 35 | 9 | 121 | 46 | 142 | 80 | 7 | 2 | 368 | 153 |

1275 FDR: false discovery rate

1276 A5SS: alternative 5' splice site

1277 A3SS: alternative 3' splice site

1278 SE: skipped exon

1279 IR: Intron retention

1280 MXE: mutually exclusive exons

1281

1282

1283 **Table 1-2.** Number of alternative splicing loci with significant difference in liver

| | SE | A5SS | A3SS | MXE | IR | Total |
|---|---|---|---|---|---|---|
| **KL+/KL-** | 121 | 35 | 63 | 7 | 142 | 368 |
| **KL+/WT+** | 222 | 37 | 59 | 6 | 90 | 414 |
| **KL+/WT-** | 199 | 31 | 43 | 7 | 59 | 339 |
| **KL-/WT+** | 294 | 67 | 121 | 16 | 382 | 880 |
| **KL-/WT-** | 205 | 36 | 77 | 9 | 212 | 539 |
| **WT+/WT-** | 90 | 23 | 25 | 5 | 56 | 199 |

1284

1285

1286

1287

1288

1289

1290 **Table 2.** Increase or decrease in IR ratio of splicing-related genes in blood, heart, kidney and liver

1291 by administration of JTT

| Gene Symbol | IR locus | Blood | Heart | Kidney | Liver |
|---|---|---|---|---|---|
| *Cdk11b* | 4:155625654-155625726 | | | | ↓ |
| *Cdk16* | X:20696836-20696921 | ↓ | | | |
| *Cdk5* | 5:24422388-24422497 | | | | ↓ |
| *Celf1* | 2:91013402-91016565 | ↓ | | | |
| *Ddx5* | 11:106782693-106783958 | ↓ | | | ↓ |
| *Hnrnpl* | 7:8818532-28818643 | | ↑ | | |
| *Nxf1* | 19:8765031-8766796 | | | | ↓ |
| *Sf3b1* | 1:55014562-55016375 | ↓ | | | ↓ |
| *Srrm1* | 4:135344669-135346734 | | | | ↓ |
| *Srsf5* | 12:80947865-80949094 | ↓ | | ↓ | ↓ |
| *Srsf6* | 2:162932142-162933425 | ↓ | | | ↓ |
| *Thoc2* | X:41822871-41823361 | | | | ↓ |
| *U2af1l4* | 7:30564101-30564202 | | | ↑ | |

1292

1293

1294

1295

1296